Biochimica et Biophysica Acta 1798 (2010) 1663–1678

Contents lists available at ScienceDirect

Biochimica et Biophysica Acta

journal homepage: www.elsevier.com/locate/bbamem

Mimicking SP-C palmitoylation on a peptoid-based SP-B analogue markedly improves surface activity

Michelle T. Dohm [a], Nathan J. Brown [b], Shannon L. Seurynck-Servoss [b], Jorge Bernardino de la Serna [c,*], Annelise E. Barron [b,d,*]

[a] Department of Chemistry, Northwestern University, Evanston, Illinois, 60208, USA
[b] Department of Chemical and Biological Engineering, Northwestern University, Evanston, Illinois, 60208, USA
[c] The MEMPHYS-Center for Biomembrane Physics, Department of Physics and Chemistry, University of Southern Denmark, 5230M Odense, Denmark
[d] Department of Bioengineering, Stanford University, Stanford, California, 94305-5440, USA

ARTICLE INFO

Article history:
Received 13 November 2009
Received in revised form 20 April 2010
Accepted 26 April 2010
Available online 11 May 2010

Keywords:
Lung surfactant
SP-B
SP-C
Peptoid
Lipid monolayer
Lipid bilayer

ABSTRACT

Hydrophobic lung surfactant proteins B and C (SP-B and SP-C) are critical for normal respiration in vertebrates, and each comprises specific structural attributes that enable the surface-tension-reducing ability of the lipid–protein mixture in lung surfactant. The difficulty in obtaining pure SP-B and SP-C on a large scale has hindered efforts to develop a non-animal-derived surfactant replacement therapy for respiratory distress. Although peptide-based SP-C mimics exhibit similar activity to the natural protein, helical peptide-based mimics of SP-B benefit from dimeric structures. To determine if *in vitro* surface activity improvements in a mixed lipid film could be garnered without creating a dimerized structural motif, a helical and cationic *peptoid*-based SP-B mimic was modified by SP-C-like *N*-terminus alkylation with octadecylamine. "Hybridized" mono- and dialkylated peptoids significantly decreased the maximum surface tension of the lipid film during cycling on the pulsating bubble surfactometer relative to the unalkylated variant. Peptoids were localized in the fluid phase of giant unilamellar vesicle lipid bilayers, as has been described for SP-B and SP-C. Using Langmuir–Wilhelmy surface balance epifluorescence imaging (FM) and atomic force microscopy (AFM), only lipid-alkylated peptoid films revealed micro- and nanostructures closely resembling films containing SP-B. AFM images of lipid-alkylated peptoid films showed gel condensed-phase domains surrounded by a distinct phase containing "nanosilo" structures believed to enhance re-spreading of submonolayer material. *N*-terminus alkylation may be a simple, effective method for increasing lipid affinity and surface activity of single-helix SP-B mimics.

1. Introduction

Lung surfactant (LS) is a functional lipid–protein mixture that coats the interior surfaces of the vertebrate lung as a film [1–4]. By reducing surface tension (γ, mN m^{-1}) throughout the respiration cycle, LS minimizes the effort in breathing and stabilizes the alveolar network against collapse. LS predominantly forms an air/liquid (a/l) interfacial monolayer, but attached bi/multilayers are created as the film surface area is expanded and compressed. The composition of LS is primarily lipid by weight (~90% including cholesterol), but the surfactant protein (SP) fraction (~5–10%) is critical for biophysical functioning [5,6]. The two hydrophobic proteins, SP-B and SP-C (~1–3 wt.% of natural LS), are lipid-associated and sustain the efficacy of the film, promoting: (i) rapid a/l interfacial adsorption, (ii) attainment of

Abbreviations: LS, lung surfactant; γ, surface tension in mN m^{-1}; SP-B, surfactant protein B; SP-C, surfactant protein C; a/l, air/liquid; SRT, surfactant replacement therapy; IRDS, infant respiratory distress syndrome; ARDS, acute respiratory distress syndrome; SP-B_{1-25}, *N*-terminus fragment of SP-B consisting of amino acids 1–25; dSP-B_{1-25}, dimeric SP-B_{1-25}; TL, Tanaka lipids, 68:22:9 [wt] DPPC:POPG:PA; DPPC, 1,2-dipalmitoyl-*sn*-glycero-3-phosphocholine; POPG, 1-palmitoyl-2-oleoyl-*sn*-glycero-3-phospho-*rac*-(1-glycerol); PA, palmitic acid; CD, circular dichroism; PBS, pulsating bubble surfactometer; GUVs, giant unilamellar vesicles; LWSB, Langmuir–Wilhelmy surface balance; FM, epifluorescence microscopy; AFM, atomic force microscopy; Boc, di-tert-butyl dicarbonate; *N*Lys, *N*-(4-aminobutyl)glycine; *N*spe, (*N*)-(*S*)-(1-phenylethyl)glycine; *N*ocd, (*N*)-(octadecyl)glycine; TFA, trifluoroacetic acid; TR-DHPE, Texas Red®, 1,2-dihexadecanoyl-*sn*-glycero-3-phosphoethanolamine, triethylammonium salt; SPPS, solid phase peptide synthesis; RP-HPLC, reverse-phase high performance liquid chromatography; ESI/MS, electrospray ionization mass spectrometry; MALDI-TOF/MS, matrix-assisted laser desorption/ionization time of flight mass spectrometry; λ, wavelength in nm; UV/Vis, ultraviolet/visible; SA, surface area; $\gamma_{eq/max/min}$, equilibrium/maximum/minimum surface tension in mN m^{-1}; π, surface pressure in mN m^{-1}; A, area in $Å^2$ per molecule; LE, liquid-expanded; LC, liquid-condensed

* Corresponding authors. A.E. Barron is to be contacted at Department of Bioengineering, Stanford University, W300B James H. Clark Center, 318 Campus Drive, Stanford, California, 94305-5444, USA. Tel.: +1 650 721 1151; fax: +1 650 723 9801. J. Bernardino de la Serna, Department of Physics and Chemistry, University of Southern Denmark, 5230 M Odense, Denmark. Tel.: + 45 6550 3510; fax: + 45 6550 4048.

E-mail addresses: m-dohm@northwestern.edu (M.T. Dohm), natebrown@u.northwestern.edu (N.J. Brown), sservoss@uark.edu (S.L. Seurynck-Servoss), joberse@memphys.sdu.dk (J. Bernardino de la Serna), aebarron@stanford.edu (A.E. Barron).

0005-2736/$ – see front matter © 2010 Published by Elsevier B.V.
doi:10.1016/j.bbamem.2010.04.012

near-zero γ at end-expiration, and (iii) re-spreading of material at the interface throughout continuous respiratory cycles. SP-B and SP-C interactions with lipids are crucial for optimal surfactant activity [7–9], as lipid-only films exhibit inferior *in vitro* and *in vivo* characteristics [10].

Surfactant replacement therapy (SRT) is the common clinical practice of animal-derived, exogenous LS administration for the treatment of infant respiratory distress syndrome (IRDS) [11]. SRTs for acute respiratory distress syndrome (ARDS) do not yet exist [12,13]. Although animal-derived SRTs have been efficacious, concerns with regard to possible zoonotic infection, and difficulties in surfactant production, such as the expense of extraction and inherent batch-to-batch variability, have spurred the research and development of synthetic formulations [14–16]. However, without SP-B, SP-C, or functional mimics thereof, these formulations will not match the performance of current SRTs. Peptoids [17], or poly-*N*-substituted glycines, have shown promise as functional mimics of SP-B and SP-C [18–23], and offer the advantages over peptides of facile synthesis [24], enhanced bioavailability and biostability through protease-resistance, and a longer shelf life with low propensity for solution-phase irreversible aggregation [25–28].

SP-B and SP-C peptide- and peptoid-based mimicry has involved targeting specific structural attributes of each protein believed to impart surface activity. SP-B is a net-cationic 79-residue monomer with three intramolecular disulfide bonds, and one intermolecular disulfide bond that homodimerizes SP-B *in vivo* [29–32]. Its unresolved structure is believed to contain four or five amphipathic helices, yielding an overall helical conformation [33]. To date, SP-B mimics have frequently represented SP-B_{1-25}, the surface-active, amphipathic, and helical *N*-terminus of the protein [34–38]. Designed sequences either exactly replicate or simplify [19,39] this segment, and in the interest of mimicking SP-B's more complex structure, dimerized versions of two amphipathic helices have been created [40,41]. With its hinge-like, cationic, and amphipathic structure, SP-B can be viewed as an interfacial lipid transporter and organizer, transiently inserting into lipid layers through Coulombic and hydrophobic interactions, and facilitating folding and re-spreading of LS material at the a/l interface.

Human SP-C is a 35-residue, extremely hydrophobic protein with a helix that closely matches the length of a DPPC lipid bilayer [32,42]. Its two adjacent cationic residues at positions 11 and 12 promote Coulombic interactions with anionic lipid headgroups [43], while the poly-valine helix and palmitoylation points 5 and 6 securely anchor it to a lipid layer [44,45]. SP-C primarily contributes to regulating the stability and viscosity [46] of the film, and its structure has indicated an ability to keep lipid bi/multilayers "attached" to the interfacial layer, thus enhancing adsorptive properties and reducing the minimum γ reached at end-expiration [47,48]. In fact, palmitoylated SP-C facilitates multilayer formation over the de-palmitoylated variant [47]. Synthesized [49–51] and recombinant [52,53] mimics of SP-C have emulated the hydrophobic helical region and palmitoylated properties of the protein with some success.

For these proteins that are difficult and impractical to synthesize or obtain in pure form on a large scale, the development of simpler molecules that replicate select structural motifs is very attractive. Peptoid-based mimics of both SP-B and SP-C have demonstrated good surface activity by specific *in vitro* tests in a tri-component lipid mixture, the Tanaka lipids (TL) [54], 1,2-dipalmitoyl-*sn*-glycero-3-phosphocholine (DPPC): 1-palmitoyl-2-oleoyl-*sn*-glycero-3-phospho-*rac*-(1-glycerol) (POPG):palmitic acid (PA) 68:22:9 [wt] [18–23,55]. To combine the attributes of these two proteins into a single mimic, and thus potentially enhance performance, the effects on *in vitro* surface activity of SP-C-like *N*-terminal mono- or di-alkylation of a helical, amphipathic peptoid-based SP-B mimic [20] were investigated.

First, we present the structural characterization of all peptoid-based mimics by circular dichroism spectroscopy (CD) and ultraviolet/visible (UV/Vis) spectroscopy. Then, the behavior of the peptoid mimics in bi/multilayer mixed lipid systems was assessed, with static and dynamic functional properties of mimics determined *via* pulsating bubble surfactometry (PBS). Lipid–peptoid interactions and phase segregation in lipid bilayers were then observed in giant unilamellar vesicles (GUVs). Further insight into interfacial lipid–peptoid monolayer behavior at the micro- and nanoscales was afforded by Langmuir–Wilhelmy surface balance studies with FM imaging (LWSB/FM), and atomic force microscopy (AFM). As the equivalent bilayer surface pressure is believed to be ~30 mN m^{-1} [56,57], the GUV bilayer technique complements studies involving FM and AFM imaging of monolayer systems at similar surface pressures. We report that the activities of the alkylated peptoids compare favorably to those of porcine-derived SP-B and the *N*-terminal fragment SP-B_{1-25}, and postulate that alkylation substantially improves surface activity by increasing lipid affinity, enhancing lipid film insertion, and contributing to the formation of submonolayer structures that aid in re-spreading lipid material at the a/l interface.

2. Materials and methods

2.1. Materials

Peptide and peptoid synthesis reagents and supplies were purchased from Applied Biosystems (ABI) (Foster City, CA) and Sigma-Aldrich (Milwaukee, WI). Fmoc-protected amino acids and resins were obtained from EMD Biosciences (NovaBiochem, San Diego, CA). Primary amines (highest purity and enantiomeric excess available, Fig. 1), di-tert-butyl dicarbonate (Boc), and palmitic acid (PA) were purchased from Aldrich. All salts, and solvents acetonitrile, 2-propanol, chloroform, methanol, and trifluoroacetic acid (TFA), HPLC grade or better, were obtained from Fisher Scientific (Pittsburgh, PA). DPPC and POPG were purchased from Avanti Polar Lipids (Alabaster, AL) and used as received. Texas Red®, 1,2-dihexadecanoyl-*sn*-glycero-3-phosphoethanolamine, triethylammoni-um salt (TR-DHPE) and 2-(4,4-difluoro-5,7-dimethyl-4-bora-3a,4a-diaza-s-indacene-3-penta-noyl)-1-hexadecanoyl-snglycero-2-phosphocho-line (Bodipy-PC) were obtained from Molecular Probes (Eugene, OR), Alexa Fluor® 633 carboxylic acid, succinimidyl ester from Invitrogen (Carlsbad, CA), and 1,1′-dioctadecyl-3,3,3′,3′-tetramethylindodicarbocyanine perchlorate [$DiIC_{18}(5)$] from Aldrich. All chemicals were used without further purification. Water was Milli-Q 18.2 mΩ cm quality.

2.2. Protein extraction, and peptide and peptoid synthesis and purification

Porcine SP-B was a gift from Prof. Jesús Pérez-Gil (Madrid, Spain), isolated from minced porcine lungs as described previously [58]. The modified peptide SP-B_{1-25} (Cys8,11 → Ala) [34,35] was synthesized by standard solid-phase peptide synthesis (SPPS) [59] Fmoc chemistry on a 0.25 mmol scale using preloaded Wang resin and an ABI 433A automated peptide synthesizer (Supplementary Material, Table 1SM). Peptoids were synthesized by the submonomer method [24] using Rink amide resin on a 0.25 mmol scale, and an ABI 433A, with Boc protection of *N*-(4-aminobutyl)glycine (*N*Lys) (Fig. 1, Table 1SM). All molecules were purified according to standard reverse-phase high performance liquid chromatography (RP-HPLC) purification techniques (see SM). Final purities were confirmed to be >97% by analytical RP-HPLC and molecular weights were obtained by either electrospray ionization mass spectrometry (ESI/MS) or matrix-assisted laser desorption/ionization time of flight mass spectrometry (MALDI-TOF/MS). Both monomer (~8794 Da) and dimer (~17,588 Da) peak intensities were observed in the MALDI-TOF/MS spectra for porcine-derived SP-B (data not shown).

Fluorescent SP-B_{1-25} and peptoids for GUV studies were prepared after synthesis and purification by adding a glycine residue spacer to

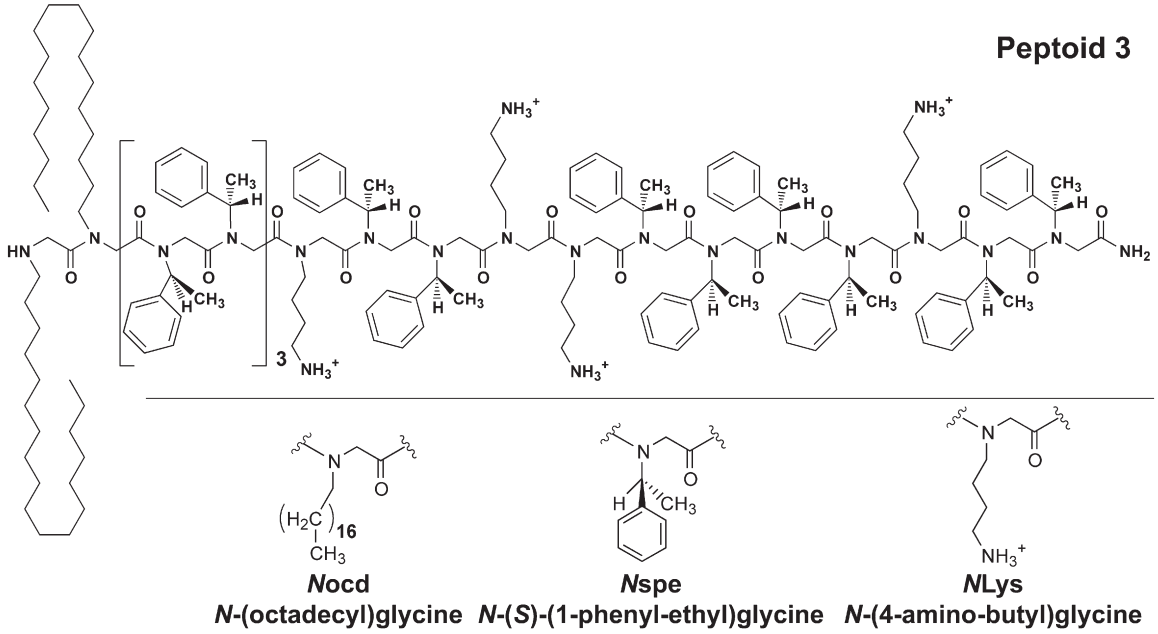

Fig. 1. Peptoid 3 chemical structure and side chain structures. Peptoid 3 is the dialkylated variant of Peptoid 1 [20]. For all peptoid sequences and molecular weights, see the Supplementary Material (Table 1SM).

activate the *N*-terminus amine, and labeling in organic solvent as described previously [60]. Briefly, ~2 mg of each molecule dissolved in a small amount of methanol was pH-adjusted to 7.0 by adding 50 mM triethylamine in methanol. The pH adjustment was necessary to deprotonate the *N*-terminus amine, allowing for preferential labeling. Each solution was then incubated in darkness at 4 °C with constant stirring in the presence of the dye Alexa Fluor® 633 carboxylic acid, succinimidyl ester for 12 h, at which point 2 M HCl was added until the pH was<3. Unreacted probe was immediately separated from the products by RP-HPLC. The labeled products were lyophilized to remove excess solvent. ESI/MS of the labeled species showed that the predominant peak was singly labeled.

2.3. Spectroscopy

Circular dichroism (CD) measurements were acquired on a Jasco J-715 spectropolarimeter (Easton, MD) in a cylindrical quartz cuvette (Hellma model 121-QS, Forest Hills, NY) with a scan rate of 100 nm min^{-1}, 0.02 cm path length, 0.2 nm data pitch, 1 nm bandwith, 2 s response, and 100 mdeg sensitivity, from wavelengths (λ) 280–192 nm. Samples were dissolved in methanol from lyophilized powder to ~15, 30, or 60 μM, calculated from averaged dry weight measurements, and run at room temperature. Alexa-labeled mimics were run at ~0.1 mg mL^{-1}. Each presented CD spectrum represents the average of 40 accumulations. Ultraviolet/Visible (UV/Vis) measurements were recorded in double beam mode on a Cary 500 UV–VIS–NIR spectrophotometer (Varian, Palo Alto, CA) using quartz cuvettes (Varian), from λ 990–190 nm with a scanning rate of 20 nm min^{-1} and data interval collection of 1 nm. Samples were dissolved in methanol from lyophilized powder to ~5, 50, or 100 μM and run at room temperature. Each UV/Vis sample was run twice.

2.4. Surfactant sample preparation

The lipids DPPC, POPG, and PA were individually dissolved in a chloroform/methanol solution (3/1 [v/v]) to ~2 or 4 mg mL^{-1}, as calculated from averaged dry weight measurements. Single-lipid solutions were then combined by volume at the ratio of DPPC:POPG:PA, 68:22:9 [wt:wt:wt] and to ~2 mg lipid mL^{-1}. This well-characterized lipid formulation, the Tanaka Lipids (TL) [54], is considered an adequate mimic of the non-protein (lipid) fraction of LS. The peptides and peptoids were individually dissolved in methanol from a lyophilized powder to ~1–2 mg mL^{-1}, as calculated from averaged dry weight measurements. For the PBS, LWSB/FM, and AFM studies, the peptides and peptoids were added to the TL lipid solution at ~2 mol% (~11–12 absolute wt.%, see Table 1SM), and the final solution was diluted to ~1 mg lipid mL^{-1}. For comparative purposes, the inclusion of peptide/peptoid at ~2 mol% corresponds to ~10 wt.% $SP\text{-}B_{1-25}$ relative to the total lipid content (~9 absolute wt.%). Porcine SP-B was dissolved in chloroform/methanol and added to the TL solution at ~1 mol%, corresponding to roughly ~10 wt.% of the monomer unit relative to the total lipid content (~9 absolute wt.%). The concentration of ~10 wt.% was selected for consistency with previous reports and to ensure comparability for all studied lipid–peptoid formulations [19–21,61–64]. GUV studies were performed with either ~5 or 10 absolute wt.% of peptide/toid. For PBS and LWSB experiments, the standard deviation of the mean (σ) was reported.

2.5. Pulsating bubble surfactometry

A commercial pulsating bubble surfactometry (PBS) instrument (General Transco, Largo, FL), modified with a direct, real-time imaging system, which has been previously described and validated in detail [63], was utilized to obtain both static-mode and dynamic-mode data. Samples were dried to a pellet from chloroform/methanol 3/1 [v/v] using a DNA 120 speedvac (Thermo Electron, Holbrook, NY). The pellet was resuspended in buffer (150 mM NaCl, 10 mM HEPES, 5 mM $CaCl_2$, pH 6.9) to ~70 μL at ~1 mg lipid mL^{-1}. Samples were mixed with a pipette 20 times, sonicated with a Fisher Model 60 probe sonicator for two 15-second spurts, and then mixed again 20 times to form a dispersed suspension. Samples were then loaded into a small plastic sample chamber (General Transco) using a modified leak-free methodology [63,65]. The sample chamber was placed in the instrument water bath at room temperature or 37 °C. A bubble with a radius of ~0.4 mm was formed, and surface area (SA) was monitored throughout the experiment (bubble size gradually increased in both data collection modes, but had a negligible effect on γ).

Static-mode adsorption data were collected for 20 min, where the suspension was allowed to adsorb to the bubble surface over time. Adsorption data were smooth fit to a curve in the Kaleidagraph®

program by applying a Stineman function to the data, where the output of this function then had a geometric weight applied to the current point and ± 10% of the data range to arrive at the smoothed curve. Dynamic-mode data were then subsequently obtained for each sample at the adult respiratory cycle frequency of 20 cycles per minute (cpm) for 10 min, with a ~50% reduction in surface area per pulsation cycle (standard for the PBS instrument). PBS experiments were repeated six times for unlabeled films at 37 °C, and three times for fluorescently labeled films at 37 °C and all films at room temperature. Representative PBS loops are presented at 5 min of cycling, and indicate clockwise bubble expansion from left to right. Percent compression is defined here as $100*[(SA_{max}-SA_{20})/(SA_{max})]$, where SA_{max} was the maximum SA value at expansion, and SA_{20} was the SA at which γ first reaches 20 mN m^{-1} upon compression.

2.6. Giant unilamellar vesicles studies

Giant unilamellar vesicles (GUVs) were prepared as previously described [66]. Initially, ~0.2 mol% of the fluorescently labeled lipid $DiIC_{18}(5)$ and either ~0.2 mol% Bodipy-PC (for lipids-only GUVs) or ~5 or 10 absolute wt.% of peptide or peptoid (for lipid–peptoid GUVs) were dissolved in methanol and added to a ~0.5 mg mL^{-1} DPPC:POPG:PA 68:22:9 [wt] lipid mixture in chloroform/methanol 3/1 [v/v]. The GUVs were produced using an electroformation method described by Angelova and Dimitrov [67,68]. Briefly, 3 μL of the labeled lipid–peptoid/tide solution was spread onto a Pt wire electrode surface in the sample well of a specially designed Teflon chamber [69], which was placed under vacuum in darkness for ≥1.5 h for trace solvent evaporation. Then, ~500 mL of a 200 mOsM sucrose solution were added to each sample well and a low frequency AC field of 10 Hz and 1.5 V amplitude was applied for 1.5 h using a function generator (Van Draper Digimess Fg 100, Stenson, Derby, UK). A circulating water bath was used to maintain the sample chamber temperature at 60 °C, sufficiently above the gel/fluid transition temperature. The GUVs were then harvested with a pipette and transferred to a plastic vial. Just prior to imaging, ~50 μL aliquots of the harvested GUV suspension were each transferred into a single well of an eight-well cell containing ~200 μL equi-osmolar glucose culture plate (Lab-Tek Brand Products, Naperville, IL). The GUVs were then imaged at room temperature, 21 °C, using an inverted confocal microscope (Zeiss LSM 510 META). The excitation wavelengths were λ~543 nm for the $DiIC_{18}(5)$ and ~633 nm for the Alexa Fluor® 663 labeled compounds.

2.7. Langmuir–Wilhelmy surface balance and epifluorescence microscopy studies

Surface pressure (π)-molecular area (A) isotherms were obtained using a custom-built Langmuir–Wilhelmy surface balance (LWSB), where the instrument and method have been previously described [19–22]. The trough was filled with ~300 mL of aqueous buffer (150 mM NaCl, 10 mM HEPES, 5 mM $CaCl_2$, pH 6.9) and heated to 25 or 37 °C. A Wilhelmy plate (Reigler & Kirstein GMBH, Berlin, Germany) was used to monitor surface pressure and calibrated in buffer before each run. Each sample was spread at the a/l interface from a 3/1 chloroform/methanol solution [v/v] using a glass syringe and allowed to equilibrate for 5–10 min. The barriers were then compressed, expanded, and compressed again at a rate of 30 mm min^{-1}. Isotherm measurements were repeated at least six times for each sample.

To record epifluorescence microscopy (FM) images, a Nikon MM40 compact microscope stand with a 100 W mercury lamp (Tokyo, Japan) was used in conjunction with the LWSB. Epifluorescence was detected by a Dage-MTI three-chip color camera (Dage-MTI, Michigan City, IN) in conjunction with a generation II intensifier (Fryer, Huntley, IL). Samples were spiked with ~0.5 mol% TR-DHPE, a fluorescently headgroup-labeled lipid, for detection. Isotherm features remained unchanged after TR-DHPE addition, and presumably, film morphology was also unchanged by the presence of TR-DHPE at these concentrations. FM images were acquired directly from the compressed film on the a/l interface. Experiments were conducted exactly as the LWSB studies of unspiked films, with the exception that barrier speed was reduced to 5 mm min^{-1}, and experiments were repeated three times. Average liquid-condensed (LC) domain sizes were calculated using ImageJ software (National Institutes of Health, Bethesda, Maryland).

2.8. Atomic force microscopy

Atomic force microscopy (AFM) results were obtained on solid-supported lipid and lipid–peptoid/tide Langmuir–Blodgett films, wherein an a/l interfacial film held at constant surface pressure was transferred onto a mica substrate. Monolayers were prepared by spreading the lipid and lipid–peptoid/tide solutions (chloroform/methanol 3/1 [v/v]) onto an aqueous-buffered subphase (150 mM NaCl and 5 mM Tris, pH 7) maintained at 25 °C in a specially designed, continuous ribbon NIMA Langmuir–Blodgett trough (NIMA Technology, UK) at minimum surface pressure (~0–1 mN m^{-1}). After 10 min of film equilibration, the monolayer was compressed at 50 cm^2 min^{-1} until the desired surface pressure was reached (~30 or 60 mN m^{-1}) (full compression isotherms are available in Fig. 7SM). The film was again equilibrated for 5 min at constant pressure. Then, a previously immersed, freshly cleaved muscovite mica substrate (Plano, Wetzlar, Germany) was vertically lifted out of the subphase at a speed of 10 mm min^{-1} to generate the solid-supported film. The deposition was complete when the substrate was completely removed from the aqueous subphase and exposed to air. The Langmuir–Blodgett film was subsequently dried overnight in a clean, sealed compartment to avoid sample contamination. Topographical images were obtained with an atomic force microscope (JPK NanoWizard, JPK Instruments, Berlin, Germany) using the air-tapping mode and Silicon-SPM cantilevers (Nanosensors, NanoWorld AG) operating at their resonance frequency (76–263 kHz) with a force constant between ~1.2 and 29 N m^{-1} (nominal). The scan rate was ~1 Hz for all experiments.

3. Results

3.1. Mimic design rationale

We aimed to mimic the helicity, hydrophobicity, and cationic facial amphipathicity of the surface-active *N*-terminus fragment of SP-B, SP-B_{1-25}, all while comprising a minimal number of different side chains, emulating KL_4 (a simplified peptide that generically adopts SP-B's overall charge patterning [39]). Minimizing the number of distinct side chains provides the advantages of ease of synthesis and reduced production costs. The design, synthesis, and *in vitro* surface activity testing of previous single-helix peptoid-based SP-B mimics have been described [19]. The *in vitro* surface activities of these peptoids in a DPPC:POPG:PA lipid film were as good as those of SP-B_{1-25} and KL_4 [19]. Particularly, the inclusion of bulky, chiral, and aromatic side chains (*N*spe, Phe-like, Fig. 1, Table 1SM) increased surfactant activity relative to sequences containing chiral, aliphatic side chains (*N*ssb, Ile-like).

A subsequent study described improved *in vitro* surface activity after including an end-on attachment of an insertion region at the *N*-terminus (Fig. 1) [20], meant to mimic SP-B_{1-9}, the flexible strand fragment considered critical for γ-reducing ability [70]. Although the hydrophobic and helical nature of the peptoid segment contrasted with the proline-containing peptide insertion region (prolines incorporate well into peptoid helices), the similarity between the sequences resided in the eight-residue length and the high proportion of ring-containing side chains in the peptide (Phe, Pro, Tyr, and Trp) known to facilitate lipid insertion [20,70].

In parallel, our development of peptoid-based SP-C mimics is ongoing [18,22], and current investigations revealed that *N*-terminus

alkylation dramatically increased *in vitro* surface activity in these mimics (submitted manuscript [71]). Therefore, in the interest of uniquely combining the functionalities of, or "hybridizing," SP-B and SP-C into a single peptoid to enhance *in vitro* performance, the most promising peptoid-based SP-B mimic, **1**, was mono- (**2**) and dialkylated (**3**) with *N*-(octadecyl)glycine (*N*ocd, or octadecylamine) at the *N*-terminus (Fig. 1, Table 1SM), and subsequent effects on activity were explored by multiple *in vitro* tests. Note that the *N*ocd submonomer is incorporated into the peptoid sequence easily using the standard submonomer synthesis method [24].

3.2. Spectroscopy

3.2.1. Circular dichroism spectroscopy

CD spectra were recorded to assess solution-phase secondary structure for all peptoids at ~60 μM in methanol, a lipid-mimetic environment, at room temperature (Fig. 2A). SP-B and its fragments are helical in solution, and the peptoids were designed to retain this characteristic in hopes of emulating the amphipathicity of the protein. All peptoids yielded spectra characteristic of aromatic peptoid helices, with a global maximum at a wavelength (λ) of ~193 nm, a minimum at ~205 nm, and a global minimum at ~221 nm [26]. The spectra of **2** and **3** directly overlaid one another (Fig. 2A). A noticeable increase in extent of helicity was observed upon alkylation in **2** and **3** relative to **1**

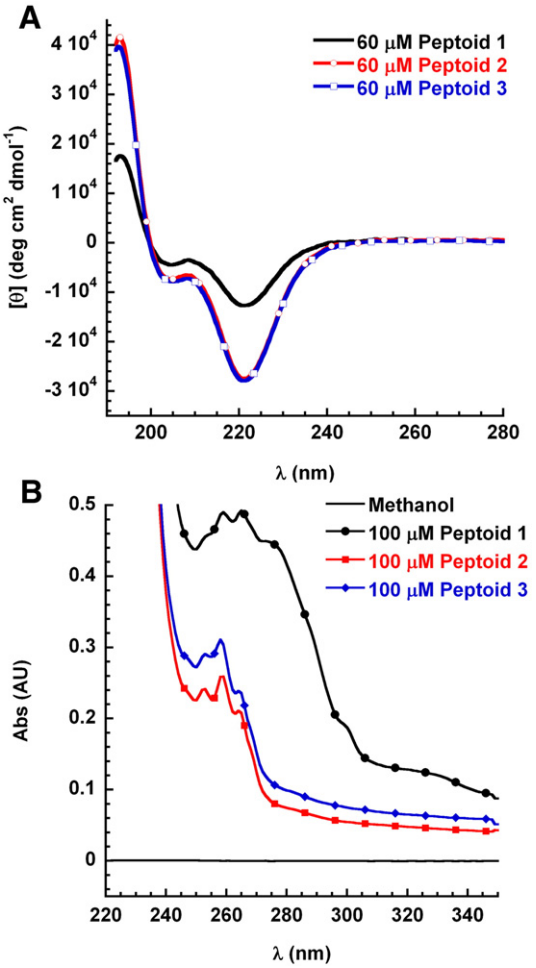

Fig. 2. CD and UV/Vis spectra of peptoids in methanol at room temperature. (A) CD spectra for peptoids in methanol at 60 μM. λ is Wavelength (nm) and θ is Per Residue Molar Ellipticity (deg cm^2 dmol^{-1}). 1 (black), 2 (red), 3 (blue). (B) UV/Vis spectra for peptoids in methanol at 100 μM. Abs is Absorbance in arbitrary units. 1 (black, circles), 2 (red, squares), 3 (blue, diamonds).

[20], particularly at the global maximum and global minimum λ (Fig. 2A). The presence and magnitude of this effect was retained over time in solution and at concentrations as low as ~30 and ~15 μM (Fig. 1SM, Panels *A*–*B*), diminishing the likelihood of a concentration-dependent associative effect. In addition, the helical nature of the SP-B$_{1-25}$ peptide (previously published) [19,20] and peptoids **1** and **3** was retained after fluorescent labeling with Alexa Fluor® 633 (Fig. 1SM, Panel C).

3.2.2. Ultraviolet/visible spectroscopy

To further explore the observed increase in extent of helicity by CD after peptoid alkylation, UV/Vis spectra were collected in methanol at room temperature, at concentrations of ~5, 50 and 100 μM (Fig. 2B and Fig. 2SM, Panel B). At all three concentrations, the spectra for **2** and **3** exhibited similar features that were different from that of **1**. At λ ~260 nm, which surveys the environment of aromatic functional groups, the peak shape was significantly broader for **1** than **2** and **3,** and an increased absorbance was observed in the light scattering range of λ 300–350 nm for **1** relative to **2** and **3**. Note that at each concentration, the λ ~260 nm absorbance for the peptoids decreased significantly in the order of **1**>**3**>**2** (Fig. 2B and Fig. 2SM, Panel B). These spectral signature changes and drop in absorption post-alkylation indicate hydrophobic interactions between the alkylated hydrocarbon chains and aromatic interactions between the amphipathic, *N*spe-containing helices. In the peptide bond-absorbing region, λ ~220 nm, **2** and **3** demonstrated much higher absorbance than **1**, indicative of a structural change in backbone amide group positioning (Fig. 2SM, Panel A). There was no evidence of micellar formation (turbidity) in the λ ~590 nm region for all concentrations tested (Fig. 2SM, Panel C).

3.3. Pulsating bubble surfactometry

3.3.1. Static-bubble mode

A functional lung surfactant must have an immediate, γ-reducing effect at an a/l interface in order to properly enable respiration. The adsorptive properties (γ vs. time) of lipid–peptoid suspensions at the interface of a ~0.4 mm radius bubble were thus monitored using the PBS at 37 °C in static-mode (Fig. 3A, representative traces). Mean $\gamma \pm \sigma$ at selected time intervals are presented in Table 1. For instance, Infasurf®, a clinically administered SRT derived from natural LS, typically reaches a low equilibrium γ (γ_{eq}) of ~23 mN m^{-1} at the a/l interface within 1–2 min on the PBS [63]. The peptoids' activities in a DPPC:POPG:PA 68:22:9 [wt] Tanaka lipid (TL) film were compared to those of porcine-derived SP-B and SP-B$_{1-25}$ in the same lipid mixture.

The TL + SP-B suspension adsorbed to γ of ~25 mN m^{-1} in less than 5 min, and attained a γ_{eq} of ~24 mN m^{-1} (Fig. 3A, Table 1). The seeming inability of TL + SP-B to reach γ_{eq} of ~24 mN m^{-1} within 1 min is likely related to either i) the lipid composition, which only partly mimics the total lipid composition of natural LS, or ii) possible localized protein aggregation due to the high content (~10 wt.%) of SP-B [72]. In stark contrast, TL adsorbed very slowly, requiring 20 min to reach a high γ_{eq} of ~53 mN m^{-1}. The TL + SP-B$_{1-25}$ film (trace not shown, previously published [19–21]) exhibited less rapid adsorption with an γ_{eq} of ~36 mN m^{-1} (Table 1). All lipid–peptoid mixtures dramatically enhanced adsorption relative to TL. As suggested by the increased σ of TL + **1** up until 10 min (Table 1), this film exhibited variable and slow adsorption rates relative to TL + **2** and TL + **3** [20]. Mono- and dialkylation improved the adsorption rate of the lipid–peptoid films, where TL + **2** and TL + **3** reached ~27 mN m^{-1} before ~2.5 min (Fig. 3A, Table 1). However, these films adsorbed to slightly higher γ_{eq}'s of ~25–26 mN m^{-1}, while TL + **1** attained a γ_{eq} of ~23 mN m^{-1}.

3.3.2. Dynamic-bubble mode

The maintenance of good surfactant activity during the dynamic changes in volume or film surface area at the a/l interface was assessed *via* bubble pulsation in PBS dynamic-mode. This method permits a simplified evaluation of *in vitro* dynamic film behavior,

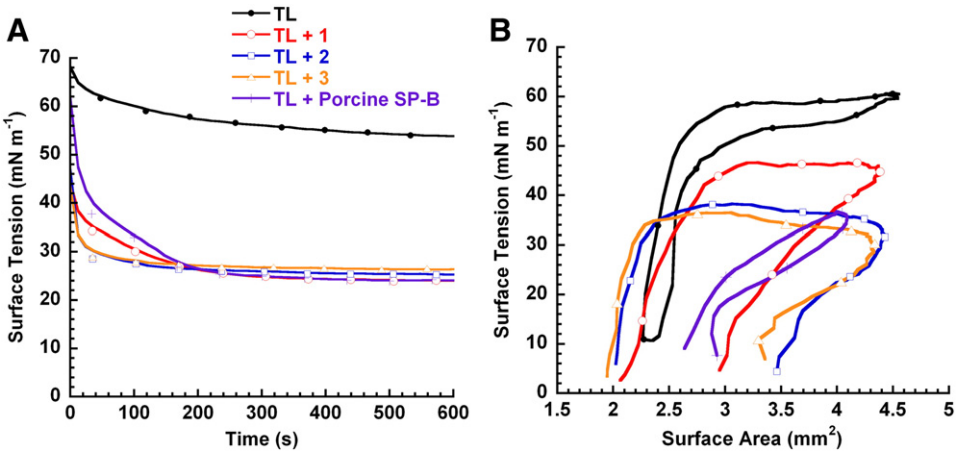

Fig. 3. PBS static- (A) and dynamic-mode (B) data for lipid–peptoid aqueous buffer suspensions at 37 °C. Tanaka lipids alone (TL, black, circles), TL + 1 (red, open circles), TL + 2 (blue, triangles), TL + 3 (orange, diamonds), and TL + SP-B (purple, vertical crosses) in aqueous buffer (150 mM NaCl, 10 mM HEPES, 5 mM $CaCl_2$, pH 6.9) at 37 °C. See Tables 1 and 2 for static- and dynamic-mode data, respectively. Data presented are representative traces, where in dynamic-mode (B), traces are after 5 min of cycling at the approximate adult respiratory rate of 20 cycles per minute (cpm), and bubble expansion is clockwise from left to right.

including the ability of a film to reach a desirable low maximum and near-zero minimum γ (γ_{max} and γ_{min}, respectively) [63]. The γ-surface area (SA) data loops in Fig. 3B for each lipid–peptoid mixture are one representative pulsation cycle at 20 cycles per minute (cpm) after 5 min at 37 °C, with bubble expansion in a clockwise loop direction. The mean $\gamma_{max/min} \pm \sigma$ at selected time intervals are presented in Table 2.

The absence of low-γ data in some loops results from the inability of the image analysis system to trace the bubble shape in this regime. The highly compressed state of the film that enables it to reach low γ often causes significant bubble shape deformation that inhibits bubble tracing to obtain SA or employing the ellipsoidal Laplace equation to calculate γ [63]. However, lipid–peptoid films that did not reach $<1\,mN\,m^{-1}$ could be accurately traced to the minimum surface tension reached and never exhibited significant bubble deformation. Visual, real-time bubble inspection confirmed that significant bubble deformation occurred and that γ reached near-zero in these films. Although bubble size varied slightly for every experiment, small differences in *x*-axis positioning (SA) had a negligible effect on γ.

The PBS cycling loop for clinically used Infasurf® has a γ_{max} of ~35 mN m^{-1} and a γ_{min} near zero [63]. This near-zero γ_{min} should appear upon cycling commencement and remain indefinitely with minimal SA compression to reach near-zero γ. Similarly, the TL + SP-B film exhibited a γ_{max} of ~36 mN m^{-1} and near-zero γ_{min}, with ~21% SA compression to reach 20 mN m^{-1} (Fig. 3B, Table 2). The TL film demonstrated very poor surfactant activity characteristics, with a high γ_{max} of ~63 mN m^{-1}, a γ_{min} of ~12 mN m^{-1}, and ~49% compression. The addition of unalkylated **1** to the lipid film reduced the γ_{max} to ~46 mN m^{-1} and the γ_{min} to near-zero immediately upon pulsation. The percent SA compression was also reduced to ~26%. The γ_{max} and percent SA compression further decreased upon mono- (**2**), and then dialkylation (**3**), of the peptoid helix, with **3** reaching a γ_{max} matching that of Infasurf® (~35 mN m^{-1}), and attaining a surprisingly low 12% SA compression to reach 20 mN m^{-1} (Table 2). Also of note are the differences in bubble shape between TL + SP-B and the TL + peptoid films, where the loop hysteresis was much larger for peptoid-containing films (Fig. 3B). The significance of a large degree of hysteresis has not yet been established, but in lipid–peptoid films generally correlates with less compression to reach near-zero γ [19,20].

In peptoids, the improved PBS activity could be associated with the amount of material attached to the monolayer and therefore available for reincorporation during the re-expansion process (inhalation) as film surface area increases. Structurally, this material would likely form bilayers, and therefore, we have employed GUVs to observe the lipid phase segregation behavior and specific lipid–peptoid interactions in these lipid bilayer vesicles.

Table 1
Summary of PBS adsorption data at 37 °C in static-mode at selected time intervals. Dried lipid–peptoid films (lipid ~1 mg mL^{-1}) were resuspended in aqueous buffer (150 mM NaCl, 10 mM HEPES, 5 mM $CaCl_2$, pH 6.9) and allowed to adsorb to the bubble interface over time. The standard deviation of the mean (σ) is reported.

Film	γ[a] 1 min		γ 2.5 min		γ 5 min		γ 10 min		γ_{eq} 20 min	
	Avg	σ	Avg	σ	Avg	σ	Avg	σ	Avg	σ
TL[b]	61.3	1.9	59.0	1.8	56.8	1.8	54.6	1.8	52.6	1.7
TL + 1[c]	33.9	5.8	29.4	4.6	26.5	3.9	23.9	1.2	23.2	0.9
TL + 2	28.6	1.1	27.1	0.5	26.3	0.6	25.5	0.7	25.3	0.9
TL + 3	27.8	0.9	27.0	0.8	26.5	0.8	25.8	0.9	25.6	1.4
TL + SP-B[d]	33.5	2.4	28.3	1.9	25.7	0.8	24.6	0.9	24.4	1.1
TL + SP-B_{1-25}	40.5	1.2	39.4	1.9	37.9	1.2	36.8	1.0	35.6	1.3

[a] Mean surface tension in mN m^{-1}.
[b] Tanaka lipid mixture, DPPC:POPG:PA 68:22:9 [wt].
[c] Mimics added at ~2 mol%, equivalent to ~10 wt.% SP-B_{1-25} peptide relative to the total lipid content.
[d] Porcine SP-B added at ~1 mol% based on monomer composition, roughly equivalent to ~10 wt.% relative to the total lipid content.

3.4. Giant unilamellar vesicle studies

The lipid phase segregation pattern in the bilayer plane was imaged in GUVs comprising TL, doped with ~0.2 mol% of the labeled lipid $DiIC_{18}(5)$ and either ~0.2 mol% of the labeled lipid BODIPY-PC (for TL-only GUVs), or ~10 absolute wt.% of fluorescently labeled SP-B_{1-25}, **1**, or **3**, (for TL + peptoid GUVs) at room temperature (Fig. 4). The labeled lipids $DiIC_{18}(5)$ and BODIPY-PC were bulky and preferentially excluded from the well-ordered lipid phases (dark), and distributed into the fluid phase (bright), providing phase coexistence contrast in the GUV images [73]. Native SP-B was previously studied using GUVs in a different lipid mixture [66], where it was determined that, in a fluid ordered/fluid disordered two-phase coexistence, SP-B co-localized with SP-C in the disordered phase. Therefore, the preferential partitioning of our mimics and SP-B_{1-25} in free-standing TL lipid bilayers is of comparative interest for this particular study.

In all images, the lipid probes resided in the fluid phase. Based on the apparent partitioning of the lipophilic probes used [73], the domain shape, and the saturated/unsaturated chain properties of the

Table 2
PBS dynamic-mode cycling data at 37 °C at selected time intervals. Dried lipid–peptoid films (lipid ~1 mg mL^{-1}) were resuspended in aqueous buffer (150 mM NaCl, 10 mM HEPES, 5 mM $CaCl_2$, pH 6.9), wherein a bubble was pulsed at 20 cpm. The standard deviation of the mean (σ) is reported.

Film	1 min				5 min				10 min				% comp[b]	σ
	γ^{a}_{max}	σ	γ_{min}	σ	γ_{max}	σ	γ_{min}	σ	γ_{max}	σ	γ_{min}	σ		
TL[c]	64.3	2.8	12.3	2.4	63.3	2.4	12.3	1.8	62.3	2.4	11.6	3.1	48.7	2.9
TL + 1[d]	44.9	1.2	<1[f]	–	46.1	1.0	<1	–	46.1	1.9	<1	–	26.4	3.6
TL + 2	38.6	2.4	<1	–	39.7	2.8	<1	–	39.8	2.6	<1	–	16.6	3.5
TL + 3	34.9	1.6	<1	–	35.2	2.0	<1	–	35.0	2.2	<1	–	12.2	3.8
TL + SP-B[e]	36.5	1.1	<1	–	35.8	1.3	<1	–	36.0	1.9	<1	–	21.0	2.6
TL + SP-B_{1-25}	49.6	0.5	<1	–	49.9	0.4	<1	–	49.8	0.7	<1	–	33.2	2.7

[a] Mean surface tension in mN m^{-1}.
[b] Percent compression is defined here as $100*[(SA_{max} - SA_{20}) / (SA_{max})]$, where SA_{max} was the maximum surface area (SA) at expansion, and SA_{20} was the SA at which γ first reaches 20 mN m^{-1} upon compression.
[c] Tanaka lipid mixture, DPPC:POPG:PA 68:22:9 [wt].
[d] Mimics added at ~2 mol%, equivalent to ~10 wt.% SP-B_{1-25} peptide relative to the total lipid content.
[e] Porcine SP-B added at ~1 mol% based on monomer composition, roughly equivalent to ~10 wt.% relative to the total lipid content.
[f] No σ values are available for "<1" table entries.

lipid components of the TL mixture, it was concluded that a gel/fluid phase coexistence occurred in all lipid and lipid–peptide/toid vesicles (Fig. 4). In the TL vesicles, rounded, gel-like, and condensed domains were surrounded by a fluid phase, whereas in TL + SP-B_{1-25} vesicles, both rounded and multi-lobed condensed domains were present. The fractal boundaries of the multi-lobed condensed domains are indicative of a highly packed structure. Interestingly, the TL + **1** vesicles consisted mostly of multi-lobed, condensed domains, while TL + **3** vesicles, like TL + SP-B_{1-25}, exhibited both rounded and smaller, multi-lobed condensed domains. In addition, the localization of SP-B_{1-25}, **1**, and **3** in the GUVs was in the fluid phase, as evidenced by the individual lipid-labeled (yellow) and peptoid-labeled (blue) image panes (Fig. 4). GUVs imaged with $DiIC_{18}(5)$ and ~5 wt.% labeled SP-B_{1-25}, **1**, or **3** (Fig. 5SM) were similar to those at ~10 wt.%, and GUVs containing $DiIC_{18}(5)$ and unlabeled SP-B_{1-25}, **1**, or **3** (Fig. 5SM) exhibited similar phase morphology to the films containing labeled variants.

Lipid films containing the Alexa-labeled variants incorporated into GUVs were also assessed utilizing the PBS to ensure that surface activity was retained after labeling (see SM for detailed results, including Figs. 3–4SM and Tables 2–3SM). Although lowered surface activity was noted in all mimics after labeling, the decreasing trend in surface activity of **3**>**1**>SP-B_{1-25} remained consistent.

3.5. Langmuir–Wilhelmy surface balance studies

3.5.1. Isotherm compression

To assess lipid–peptoid surface activity in a monolayer system and compare behavior to films containing the peptide and natural protein, isotherms and FM images were recorded for all lipid–peptoid formulations. Surface pressure (π, mN m^{-1}) — molecular area (A, Å^2 molec^{-1}) representative first compression and expansion isotherms (Figs. 5 and 6, respectively) and representative FM images (Fig. 5) for TL + peptoid films spread at the a/l interface were obtained on a custom-built LWSB and performed at 25 and 37 °C. For 25 °C compression isotherms and FM images, see Fig. 6SM. The isotherm features of the TL + peptoid films herein were compared to TL + SP-B and TL + SP-B_{1-25} films (Fig. 5, Table 3). For mean liftoff data and 2D first compression isotherm features $\pm\sigma$, at both 25 and 37 °C, see Table 3.

For the TL + SP-B film at 37 °C (Fig. 5, Table 3), the isotherm exhibited a desirable early (high) 'liftoff' area, or the A at which π first measurably increases from zero. After a procession from the liquid-expanded (LE) to liquid-condensed (LC) phases, the film reached a high collapse π of ≥70 mN m^{-1} that indicates an ability to reach near-zero γ (Fig. 5). The magnitude of the increase in liftoff A with an additive, relative to the lipid-only film, correlates with the molecule's ability to crudely organize an adsorbed interfacial structure. This effect is recognized by a measurable increase in π, and is considerably

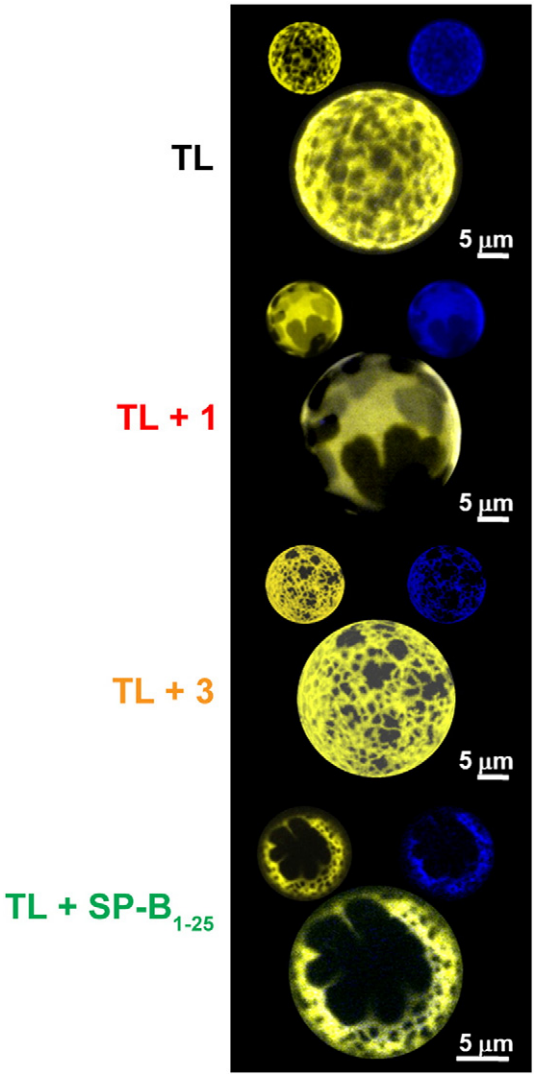

Fig. 4. Lateral distribution of peptide-/peptoid-based mimics in DPPC:POPG:PA giant unilamellar vesicles (GUVs) at room temperature. The vesicles were spiked with the lipophilic fluorescent probes $DiIC_{18}(5)$ and Bodipy-PC, and SP-B_{1-25} and peptoids were fluorescently tagged with Alexa Fluor® 633 carboxylic acid, succinimidyl ester. SP-B_{1-25} and peptoids were present in films at ~10 wt.%. For TL, TL + 1, and TL + 3, the larger vesicle is a 3D reconstruction image, while the TL + SP-B_{1-25} large vesicle is from the polar region of the vesicle. To the upper left of each large vesicle (combination image) is the lipid-only image pane (yellow, $DiIC_{18}(5)$), and to the upper right is the peptoid-only image pane (blue, Alexa 633), except in the case of TL, for which it is BODIPY-PC pane. Scale bars correspond to 5 µm.

affected by the additive size, which alters the available area per molecule (A). In addition, a pronounced, extended plateau occurred at ~40–50 mN m^{-1} in TL + SP-B films (Fig. 5). Changes in monolayer/multilayer structure in the plateau region are still well-debated, but the plateau's presence is a defining characteristic of SP-B- and SP-C-containing films, and corresponds to reversible exclusion ("squeeze-out") of material from the monolayer into attached structures below or above the surface. The isotherm for TL + SP-B$_{1-25}$, previously published [19–21], exhibited a later liftoff area than TL + SP-B with a less pronounced plateau at both temperatures (Table 3), a result likely due to the smaller size of the molecule as well as a decrease in biomimetic behavior relative to the full-length protein.

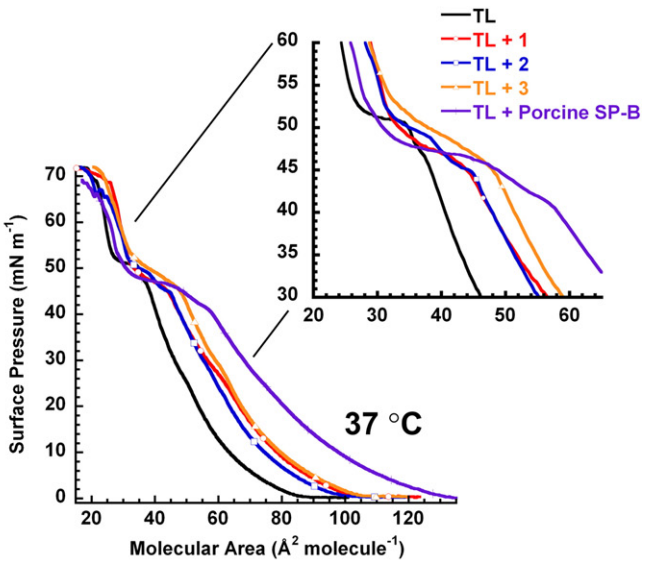

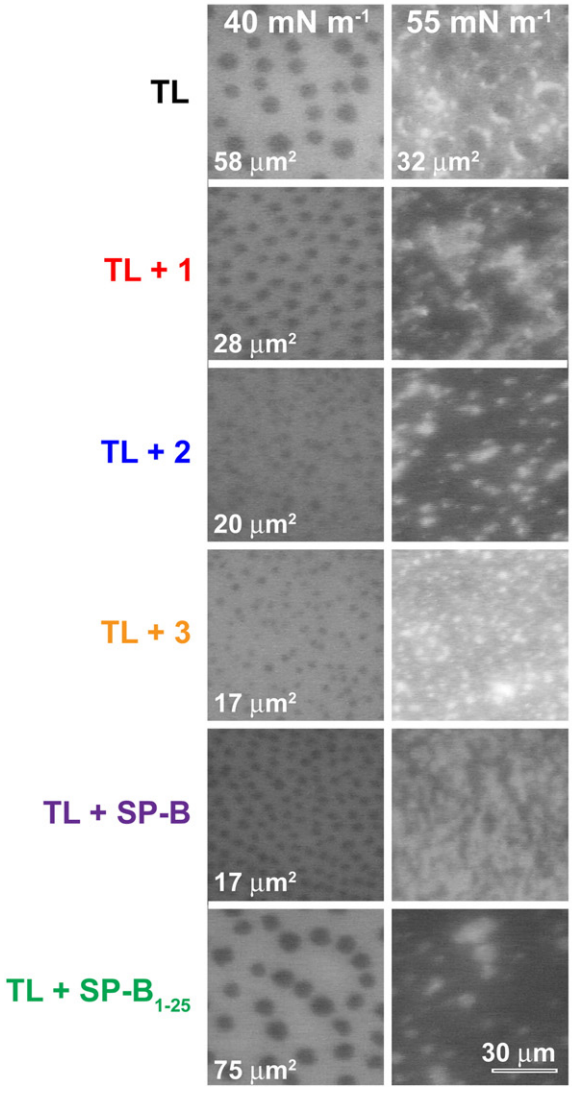

At 37 °C, all films exhibited a high collapse of $\pi \geq 70$ mN m^{-1}. The TL film exhibited a later liftoff and less pronounced plateau than any of the lipid–peptoid films (Table 3), while TL + SP-B demonstrated the earliest liftoff and most pronounced plateau. All TL + peptoid isotherms had earlier liftoff areas relative to the TL only film, indicating increased surface activity and the presence of an additive [19,20]. The isotherm features for all three lipid–peptoid films were similar until the plateau region (Fig. 5). However, distinct differences were apparent in plateau region size and shape, where TL + **3** had the most pronounced plateau, second only to TL + SP-B (Table 3). All first compression isotherm trends and features observed at 37 °C were also apparent at 25 °C (Table 3, Fig. 6SM).

3.5.2. Epifluorescence microscopic imaging

Comparative insight into the 2D phase morphology and lipid–peptoid interactions in the plateau region, relative to the peptide and the natural protein, was obtained by recording FM images with ~0.5 mol% TR-DHPE spiked into the TL or TL + peptoid solution, and are presented at ~40 and 55 mN m^{-1} (below and above the plateau region), respectively, at 37 °C (Fig. 5) and ~30 and 60 mN m^{-1}, respectively, at 25 °C (Fig. 6SM). TR-DHPE is a bulky, fluorescently headgroup-labeled lipid that is size-excluded from the ordered phase of the monolayer upon sufficient lipid packing during film compression. Therefore, apparent dark regions of the monolayer correspond to liquid-condensed (LC) domains, while brighter regions represent the disordered liquid-expanded (LE) phase. Particularly bright spots in images signify sub- or super-monolayer protrusions of unknown composition that are excluded from, yet still associated with, the monolayer, known here as "bright protrusions."

In these films, LC domains formed at 6–7 mN m^{-1} at 25 °C and 28–35 mN m^{-1} at 37 °C; bright protrusions, if present, occurred at 46–48 mN m^{-1} at both 25 °C and 37 °C. Below the plateau regime at ~40 mN m^{-1} and 37 °C, the most perceptible lipid phase morphology differences among films were in the size of the dark LC domains surrounded by the brighter fluid LE phase (Fig. 5). The LC domains in the TL film were ~58 μm^2 in area, with larger LC domains for TL + SP-B$_{1-25}$ (~75 μm^2) and the other films ranked in the order of decreasing LC domain size **1**>**2**>**3**≅SP-B. In some experimental runs, the LC domains for **2** and **3** were very difficult to image due to their small size. At ~55 mN m^{-1}, the TL film retained smaller size and density LC domains than at ~40 mN m^{-1} (~32 μm^2), with the added presence of bright protrusions residing in the LE phase. In contrast, the LC domains in the lipid–peptoid and lipid-SP-B/SP-B$_{1-25}$ films at ~55 mN m^{-1} seemed quite sparse or absent (Fig. 5). The disappearance of LC domains at physiological temperature has been previously observed in other lipid films containing aromatic peptoids [19].

Fig. 5. LWSB surface pressure (π)–molecular area (A) compression isotherms and FM images at 37 °C. π–A isotherms are representative first compressions of a spread film on aqueous buffer (150 mM NaCl, 10 mM HEPES, 5 mM $CaCl_2$, pH 6.9) with a unidirectional barrier speed of 30 mm min^{-1}. Tanaka lipids alone DPPC:POPG:PA (68:22:9 [wt]) (TL, black), TL + 1 (red, circles), TL + 2 (blue, squares), TL + 3 (orange, triangles), and TL + SP-B (purple, crosses). See Table 3 for isotherm 2D phase transition markers. FM images for TL and TL + 1, 2, 3, SP-B$_{1-25}$, or SP-B are presented on the right at ~40 and 55 mN m^{-1} at 37 °C. To record images, films were spiked with ~0.5 mol% TR-DHPE and compressed at a barrier speed of 5 mm min^{-1}. Peptoids are present at ~2 mol% in the lipid film, which corresponds to ~10 wt.% SP-B$_{1-25}$ relative to the total lipid content. Porcine SP-B is present at ~1 mol% based on the monomer composition, which corresponds to ~10 wt.% relative to the total lipid content.

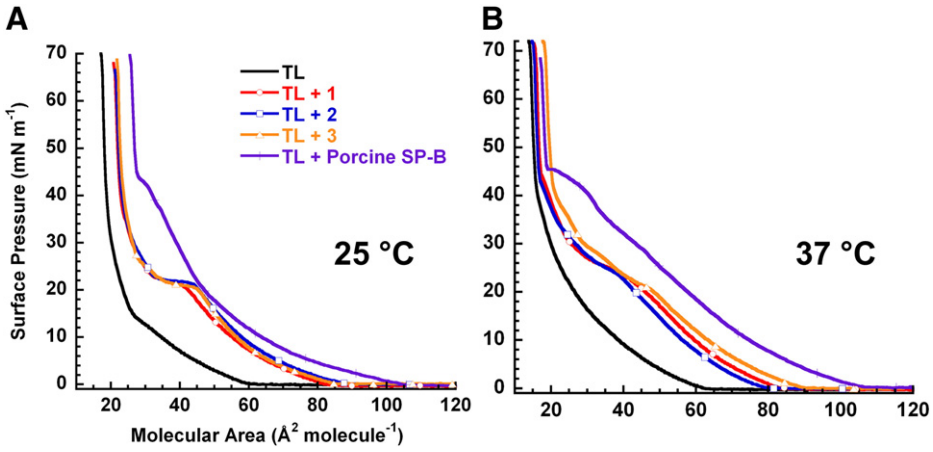

Fig. 6. LWSB surface pressure (π)–molecular Area (A) expansion isotherms at 25 °C (A) and 37 °C (B). π–A isotherms are representative first film expansions after compression to 70 mN m^{-1} on aqueous buffer (150 mM NaCl, 10 mM HEPES, 5 mM $CaCl_2$, pH 6.9) with a unidirectional barrier speed of 30 mm min^{-1}. Tanaka lipids alone DPPC:POPG:PA (68:22:9 [wt]) (TL, black), TL + 1 (red, circles), TL + 2 (blue, squares), TL + 3 (orange, triangles), and TL + SP-B (purple, crosses).

Interestingly, the TL + SP-B film displayed clustered dark areas, possibly due to interfacial SP-B protein aggregation [72], than a typically rounded or multi-lobed lipid-only LC domain (Fig. 5). The other significant changes in lipid phase morphology at higher π were evident in the bright protrusion formation and patterning, which for TL + **1**, were rather clustered in aggregate-like structures, for TL + **2,** were more distinctly rounded and separated protrusions, and for TL + **3**, were very bright and more evenly dispersed in round protrusions (Fig. 5). In TL + SP-B_{1-25}, the bright protrusions were the sparsest. The bright protrusions in TL + SP-B were more continuously clustered between dark regions and not identified as particularly bright and round-shaped as in TL + **3**. At 25 °C (Fig. 6SM), LC domains were larger and remained throughout the entire isotherm, as is expected given the higher state of meso-crystallinity in the film. In addition, at this temperature, less bright protrusion formation was observed for the TL + SP-B_{1-25} and TL + SP-B films relative to the lipid–peptoid films.

Table 3
LWSB first compression isotherm 2D phase transition markers. Mean π–A isotherm data from first compressions of a spread film on aqueous buffer (150 mM NaCl, 10 mM HEPES, 5 mM $CaCl_2$, pH 6.9) with a unidirectional barrier speed of 30 mm min^{-1}. Standard deviation of the mean (σ) is reported. Liftoff is defined as the molecular area (A) at which the surface pressure (π) first measurably increases from zero to 1 mN m^{-1}.

Film	25.0 ± 1.5 °C					37.0 ± 1.9 °C				
	Liftoff	Kink		Plateau length		Liftoff	Kink		Plateau length	
	(A[a])	(A)	(π[b])	(A)	(π)	(A)	(A)	(π)	(A)	(π)
TL[c]	$84_{(4)}$	63	5	5	7	95	49	26	11	11
TL + 1[d]	107	79	6	7	8	113	60	27	14	11
TL + 2	$109_{(3)}$	81	5	9	9	110	62	26	14	10
TL + 3	107	79	5	10	10	$116_{(5)}$	$63_{(5)}$	26	17	11
TL + SP-B[e]	120	94	5	$11_{(3)}$	10	$132_{(5)}$	69	26	$24_{(3)}$	12
TL + SP-B_{1-25}	114	92	4	11	11	$118_{(5)}$	64	25	13	13
σ[f]	≤2	≤3	≤1	≤2	≤2	3	≤3	≤2	≤2	1

[a] Mean molecular area expressed in $Å^2$ per molecule.
[b] Mean surface pressure expressed in mN m^{-1}.
[c] Tanaka lipid mixture, DPPC:POPG:PA 68:22:9 [wt].
[d] Mimics added at ~2 mol%, equivalent to ~10 wt.% SP-B_{1-25} peptide relative to the total lipid content.
[e] Porcine SP-B added at ~1 mol% based on monomer composition, roughly equivalent to ~10 wt.% relative to the total lipid content.
[f] For clarity, the standard deviation of the mean (σ) for each type of value is collectively reported at the base of the column, with exceptions in the table listed as "$x_{(y)}$," where x is the mean and y is the σ.

3.5.3. Isotherm expansion

Lipid–peptoid interactions were also monitored upon film expansion in a monolayer system, where isotherms were collected after the first compression to ~70 mN m^{-1}, and are presented as representative expansion isotherms at 25 and 37 °C (Fig. 6). At 25 °C (Fig. 6A), the TL film exhibited a small kink at 18 ± 5 mN m^{-1}, while the TL + SP-B film had a brief "plateau region" at 44 ± 2 mN m^{-1} and a small kink at 23 ± 1 mN m^{-1}. However, the TL + peptoid isotherms were similar with very pronounced plateaus beginning at ~25 mN m^{-1} and ending at ~20 mN m^{-1}. This type of "plateau" has been suggested to be a phase transition representing peptide reinsertion into the lipid film [70], and is indicative of lipid–peptoid structural reorganization at the interface. At 37 °C (Fig. 6B), the TL and TL + SP-B expansion isotherms were very similar to those at 25 °C. Interestingly, the pronounced plateau in the three TL + peptoid films at 25 °C became longer and more gradual at 37 °C, extending from ~43 mN m^{-1} to ~ 20 mN m^{-1}, which more closely resembled that of the TL + SP-B film. The reinsertion of material to the interface is critical for sustained surface activity of the LS film [70], and it was evident that the temperature (and hence fluidity) of the lipids significantly affected the "plateau" shape and thus the mechanism of material reincorporation back into the film.

3.6. Atomic force microscopy studies

Information about the lipid–peptoid interfacial mechanism of action at the quasi-molecular level, relative to films containing SP-B_{1-25}, was obtained by performing AFM on Langmuir–Blodgett lipid–peptoid films. The lipid phase morphologies of the lipid–peptoid films were characterized below and above the plateau region, 30 and 60 mN m^{-1}, respectively, by solid-supported AFM at room temperature (images and height profiles in Figs. 7–9). Imaging of the TL film at 30 mN m^{-1} (Fig. 7A) displayed a two-phase gel/fluid coexistence of both medium and large condensed-phase (LC) domains that protruded ~0.5–1.0 nm in height above the continuous, interconnected fluid (LE) phase. These findings are in good agreement with the FM images in Fig. 6SM and previous AFM work with a similar lipid mixture [74]. Some LC domains appeared to be touching or "fused," and the boundary regions of the LC domains appeared perforated with "holes" that were not visible in FM images (Fig. 6SM). The TL + SP-B_{1-25} image at 30 mN m^{-1} (Fig. 7A) also comprised large, multi-lobed LC domains that were fused and protruded ~0.5–1.0 nm above the fluid phase, but lacked the "holes" in the domain boundary regions observed in TL films. In addition, numerous small condensed-phase structures (~50–200 nm in diameter and ~0.5–1.0 nm in height) were observed in the fluid phase of the TL + SP-B_{1-25} film

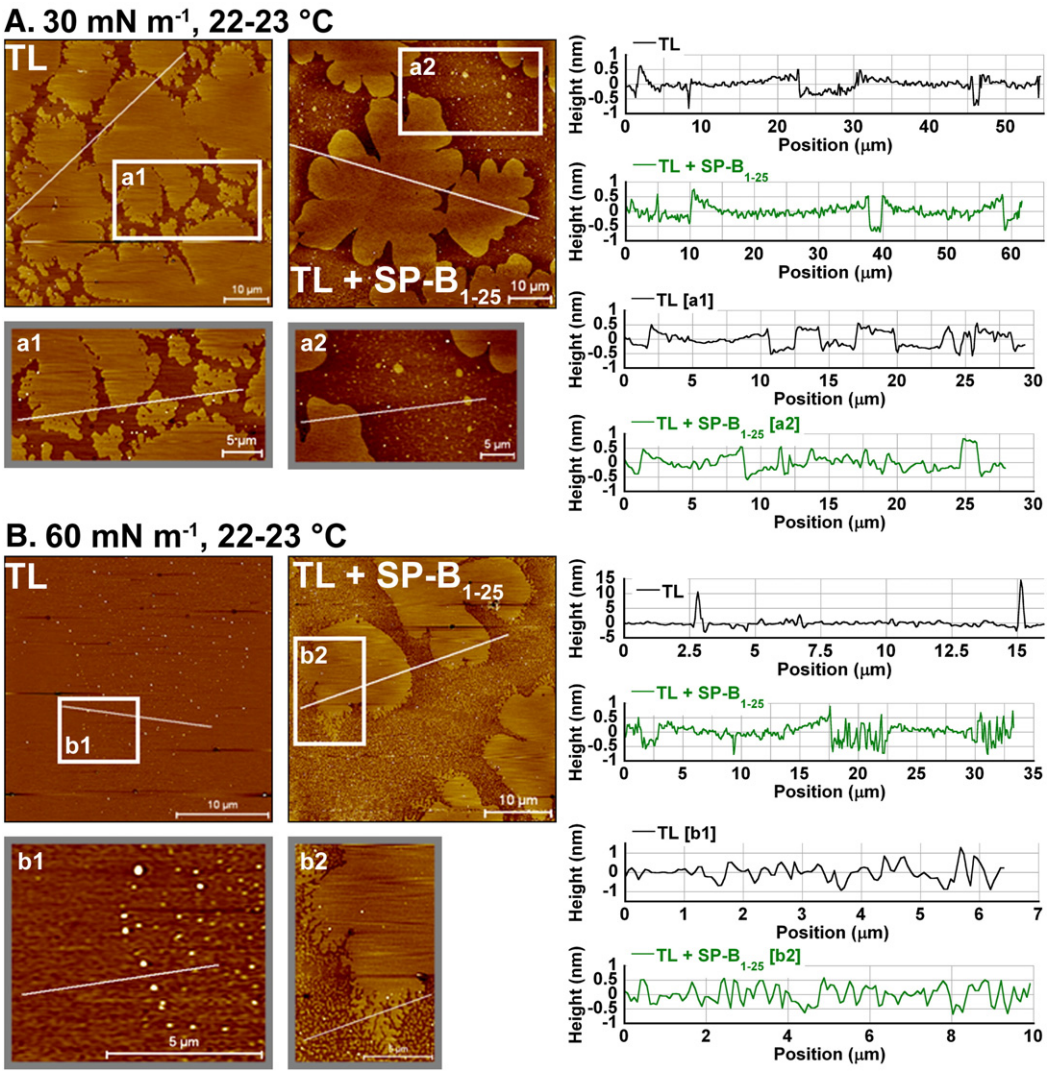

Fig. 7. Atomic force micrographs and height profiles of TL and TL + SP-B_{1-25} on mica surfaces at 30 mN m^{-1} (A) and 60 mN m^{-1} (B) at room temperature. Tanaka lipids alone DPPC:POPG:PA (68:22:9, wt) (TL, black) and TL + SP-B_{1-25} (green) monolayers spread on aqueous buffer (150 mM NaCl and 5 mM Tris, pH 7.0) were compressed to the desired surface pressure and deposited on a mica substrate for imaging. Thin white lines across each image trace the path of the height profile from left to right. Boxed in areas of 10 µm-scale images were re-imaged at the 5 µm-scale according to the lettered insets of each box. Images (left) are adjacent to corresponding height profiles (right).

(Fig. 7A, a2), but were sparsely present in the TL-only film. These nanometer-scale structures were also previously observed in films containing DPPC:POPG:PA and dSP-B_{1-25} [74].

The TL + **1** film at 30 mN m^{-1} (Fig. 8A) contained multi-lobed LC domains, smaller than those of TL + SP-B_{1-25}, that were sometimes fused and also protruded ~0.5–1.0 nm above the LE phase. Interestingly, a marked increase in the number and density of small condensed-phase structures was observed for this film. This trend continued after *N*-terminus peptoid monoalkylation (TL + **2**) (Fig. 8A), where the large LC domains were not fused and smaller than in the TL + **1** film, and more numerous, but smaller condensed-phase structures were observed. In the TL + **3** image (Fig. 9), the large LC domains were yet smaller, not fused, and surrounded by innumerous tiny condensed-phase structures throughout the fluid phase.

AFM images of Survanta® (a bovine-extracted SRT) and DPPC:POPG:PA films were hypothesized to contain "nanosilos," or small pockets of clustered material (~50–300 nm in diameter, 5–8 nm in height) that formed above the plateau region and were believed to trap material (POPG and/or SP-B) that would otherwise be lost to the subphase during compression [74]. This effect was only visible when both POPG and dSP-B_{1-25} were present, and we therefore hypothesize that the small condensed-phase structures (~1 nm in height) in the images at 30 mN m^{-1} represent nucleation points for the development of nanosilos at higher surface pressures.

Above the plateau region at 60 mN m^{-1}, a height difference no longer existed between the condensed (gel) and interconnected (fluid) phases of the TL film (Fig. 7B), and small protrusions (~10–15 nm in height) in the surrounding phase flanked the shape of the LC domains in the images. In contrast, a height difference of ~0.5–1.0 nm between the condensed and surrounding phases of TL + SP-B_{1-25} persisted at 60 mN m^{-1} (Fig. 7B), and, though the presence of many small condensed-phase structures was visible, they did not share the height characteristics (~1 nm vs. ~5–8 nm) of previously observed nanosilos [74]. The boundaries of the LC domains also became fractal-like for the TL + SP-B_{1-25} film at 60 mN m^{-1} (Fig. 7A).

The TL + **1** film resembled that of TL at 60 mN m^{-1} (Fig. 8B), where the presence of small aggregates (~12–20 nm in height) flanked the LC domains, with no appreciable height difference between the continuous phase and the LC domains. The nanosilo-like aggregates also appeared to be larger in diameter than those in the TL film. However, in TL + **2**, a distinct change in patterning occurred that resulted in two differentiated regions. Here, large, multi-lobed LC

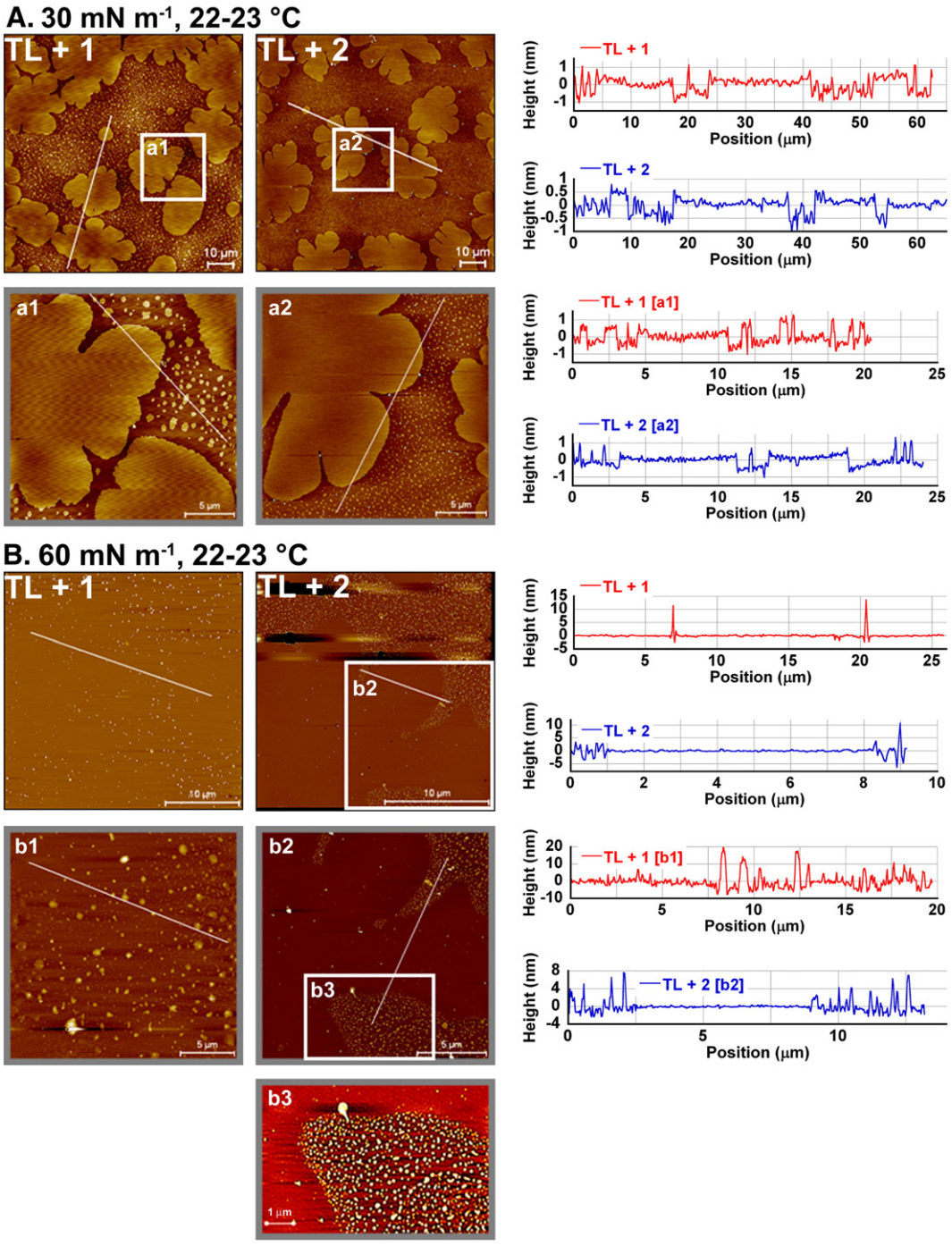

Fig. 8. Atomic force micrographs and height profiles of TL + 1 and TL + 2 on mica surfaces at 30 mN m^{-1} (A) and 60 mN m^{-1} (B) at room temperature. TL + 1 (red) and TL + 2 (blue) monolayers spread on aqueous buffer (150 mM NaCl and 5 mM Tris, pH 7.0) were compressed to the desired surface pressure and deposited on a mica substrate for imaging. Thin white lines across each image trace the path of the height profile from left to right. Boxed in areas of 10 µm-scale images were re-imaged at the 5 µm-scale and/or 1 µm-scale according to the lettered insets of each box. Images (left) are adjacent to corresponding height profiles (right).

domains were surrounded by a phase containing smaller (~2–10 nm in height), high-density nanosilos that were more uniform in shape than those present in the TL + **1** film (Fig. 8B).

In TL + **3** (Fig. 9A), the LC domain size and shape at 30 mN m^{-1} were mostly retained upon compression to 60 mN m^{-1}, again with no appreciable height difference between the condensed and surrounding phases. Instead, two differentiated regions again persisted, with innumerous nanosilos (~2–8 nm) present in the surrounding phase that were larger in diameter and present at a higher density than those in TL + **2**.

4. Discussion

The present work expands on the traditional approach to sequence design of SP-B and SP-C peptidomimetic agents by incorporating structural attributes from both proteins into one mimic. Herein, we demonstrated that the SP-C-like *N*-terminus alkylation with octadecylamine of an aromatic, SP-B-like amphipathic peptoid helix noticeably improved *in vitro* surface activity performance in a tri-component lipid film, likely through improved insertion ability, or 'anchoring' of the peptoids to the film by the octadecyl alkyl chains.

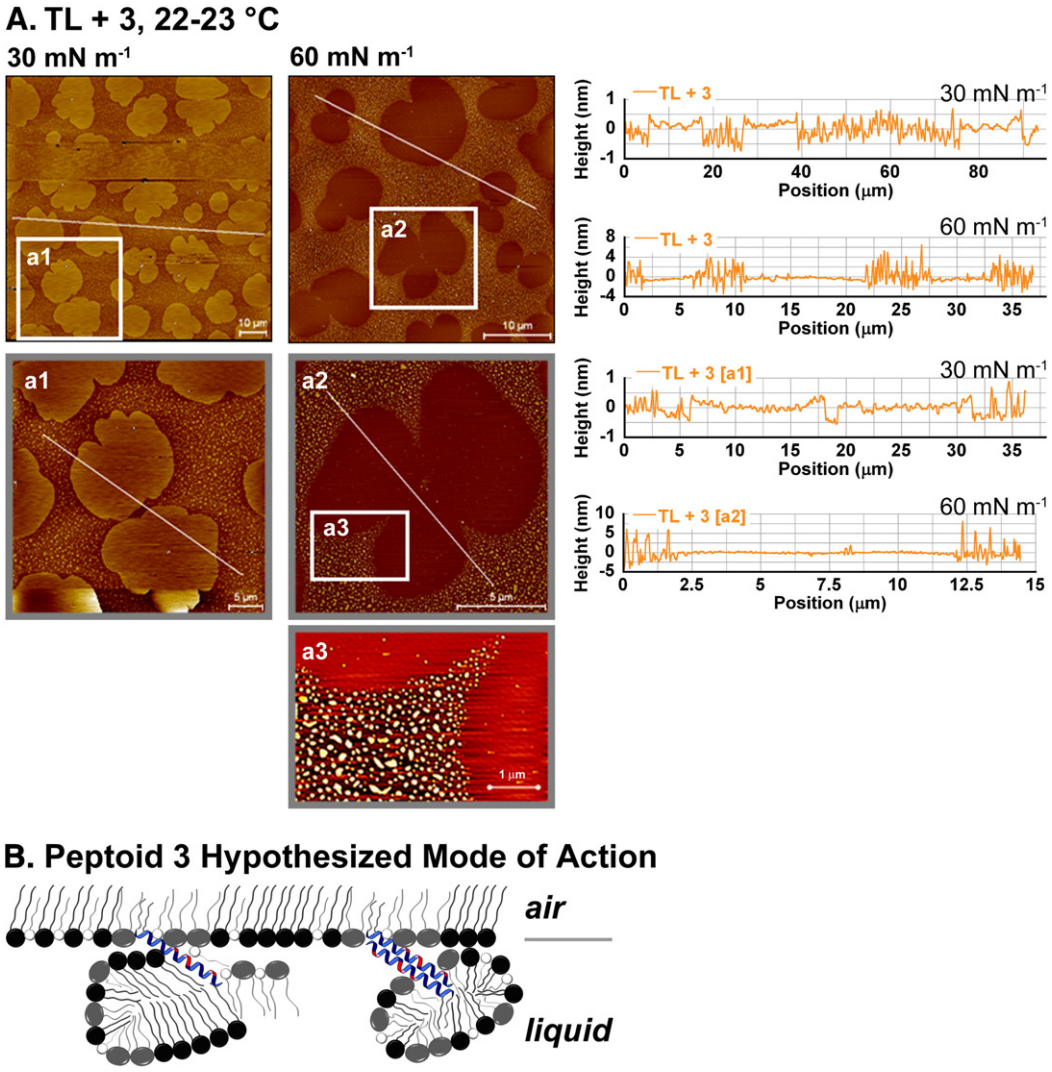

Fig. 9. Atomic force micrographs and height profiles of TL + 3 on mica surfaces at 30 mN m^{-1} and 60 mN m^{-1} at room temperature (A), and hypothesized mode of lipid–peptoid interaction (drawing) (B). A TL + 3 (orange) monolayer spread on aqueous buffer (150 mM NaCl and 5 mM Tris, pH 7.0) was compressed to the desired surface pressure and deposited on a mica substrate for imaging. Thin white lines across each image trace the path of the height profile from left to right. Boxed in areas of 10 μm-scale images were re-imaged at the 5 μm-scale and/or 1 μm-scale according to the lettered insets of each box. Images (left) are adjacent to corresponding height profiles (right). In the graphic, black circles represent DPPC, gray circles represent POPG, and white circles represent PA in the TL lipid mixture DPPC:POPG:PA 68:22:9 [wt]. The 'insertion region' of the peptoid helix inserts into the interfacial lipid monolayer, with the *N*ocd hydrocarbon chains associating with the lipid acyl chains, and the amphipathic helix (red indicates cationic regions) associating with the anionic lipid headgroups, sublayer lipid structures, and the aqueous buffer liquid subphase.

This is the first known instance of combining or "hybridizing" structural motifs of SP-B and SP-C into one mimic to enhance surfactant formulation performance. In this work, we demonstrate that alkylated peptoid-based SP-B mimics substantially improved on all three criteria considered essential to LS activity: rapid adsorption, reduction in surface tension, and sustained surface activity through multiple pulsation cycles, indicating that material is effectively re-spread.

The increase in surface activity of **2** and **3** relative to **1** correlated with an increase in extent of helicity (CD) in lipid-mimetic solvent (Fig. 2A). It is not uncommon for attachment of a fatty acid chain in peptides to increase helicity [75,76] by increasing the helical stability *via* hydrophobic chain–peptide helix interactions. Because the UV/Vis absorbance at λ ~ 260 nm resulted solely from the aromatic *N*spe side chains in the peptoid helix, the decreased absorbances at λ ~ 260 nm for **2** and **3** relative to **1** (Fig. 2B and Fig. 2SM, Panel B) could be similar to that which occurs between double-stranded and denatured DNA [77]. Alkylated peptoids may engage in intermolecular hydrophobic interactions that facilitate intermolecular aromatic residue 'stacking,' in turn causing peptoid self-assembly that 'buries' the aromatic residues and lowers UV absorbance. These peptoid–peptoid associations may stabilize the helical motif and impart surface activity to a surfactant film. Assembled alkylated peptoids could collectively anchor excluded material to the interfacial monolayer *via* multiple alkyl chains, thereby increasing adsorptive properties and facilitating re-spreading of material.

In this work, the post-alkylation ability of the lipid–peptoid mixtures to increase the adsorption rate and promote surface tension reduction were evaluated using the PBS. A setback in **1**'s surface activity was the variable, slow adsorption rate in static-mode relative to aliphatic peptoid variants [20]. The two-step process of LS adsorption comprises an initial, interfacial adsorption of dispersed surfactant, followed by film perturbation and reorganization as new material (ruptured liposomes) is added [78]. The adsorption rates of **2** and **3** were distinctly improved after an increase in aliphatic hydrophobicity *via* alkylation, suggesting an improved two-step adsorption rate. The hydrophobic, surface-active peptoids would be

attracted to the interface in an aqueous buffer environment, and the increased associative properties of the alkylated peptoids (as evidenced by UV/Vis) may further facilitate rapid adsorption.

The SP-B-containing film's seemingly slower adsorption rate could be caused by a decrease in the rate of diffusion to the interface with the increase in molecular size, or by possible interfacial protein aggregation. In previous reports, a "solubility limit" of 2 wt.% was suggested for SP-B at the interface, after which, at higher concentrations, evidence of interfacial protein aggregation was observed [72]. Although no macro-scale aggregation clusters were observed during real-time PBS bubble monitoring, strong protein associations could have significantly affected SP-B's behavior in this lipid system. A peptoid concentration-dependent surface activity study will be pursued to optimize the formulation, but for consistency in this work, the comparison of lipid–peptoid to lipid-SP-B films at similar mass concentrations was useful and necessary.

Maintaining a reduced γ_{max} throughout respiration and near-zero γ_{min} upon film compression is critical for a functional LS replacement. All lipid–peptoid films reached near-zero γ_{min} immediately upon bubble pulsation, and retained this value for the time tested. Seemingly, the importance of near-zero γ_{min} at minimum SA is often over-emphasized relative to a reduced γ_{max} at maximum SA; for instance, two surface-active peptide mimics KL_4 and SP-B_{1-25} exhibited γ_{max} values in the 48–50 mN m^{-1} range in a TL film [19]. The γ_{max} and percent compression to reach 20 mN m^{-1} of the film containing **1** were vastly improved upon alkylation, with additional incremental improvements for mono- and dialkylation that matched values obtained for the TL + SP-B film, thus surpassing the surface activity of all single helix peptide- and peptoid-based SP-B mimics developed to date. Although the hysteresis and loop shape of the lipid–peptoid films appeared considerably different from that of TL + SP-B, they coincided with a reduced percent compression that is needed for good surfactant activity. The improved PBS activity post-alkylation could be attributed to the increased lipid affinity and insertive ability of the alkylated peptoids, which may have aided in retaining material at the interface for re-spreading. We further explored this possibility by assessing lipid–peptoid interactions in several additional *in vitro* assays.

SP-B and SP-C, and peptide mimics thereof, are known to reside in the more disordered phase of a free standing lipid bilayer (GUV) [66,79–81]. We provided evidence that this is also the case for peptoids in a mixed lipid bilayer, supporting the idea that peptoids play a critical role in enhancing the adsorptive and re-spreading properties of the film *via* reinsertion of excluded material from the disordered phase. The cationic peptoid helices would likely reside in the fluid phase due to the disordered lipid packing and the anionic character of this POPG-enriched region. In addition, lipid–peptoid GUVs formed a gel/fluid phase coexistence at 30 mN m^{-1}, and although the significance of variations in gel-phase domain shape of GUVs is not yet well understood, it was visually observed that vesicles with **3** displayed similar phase segregation patterning to those with SP-B_{1-25}, possessing both multi-lobed and rounded domains. This is in contrast to the small rounded domains in the TL vesicles and the predominantly multi-lobed domains of the vesicles containing **1**. It could be hypothesized that the more rigid, aromatic-rich peptoid helix is not as well incorporated into the hydrophobic lipid acyl chains of the bilayer, and dialkylation increases peptoid affinity with the fluid phase, thereby affecting lipid phase segregation and patterning. Regardless, the inclusion of peptoids clearly had an effect on the bilayer phase segregation patterning that was distinctly different in their absence.

It should be noted that because the PBS surface activity of the Alexa-labeled variants did not match that of the unlabeled peptide/toids, caution must be used when making broad surface activity comparisons. However, the observations that trends in PBS *in vitro* surface activity among labeled variants remained the same as unlabeled variants, and that GUV phase morphologies remained unchanged in the presence of unlabeled variants, provides confidence in the reliability of these measurements.

Information about the ability of peptoids to insert into interfacial films, to affect segregation pattern morphology, and to increase tension-active properties were obtained through quasi-equilibrium compression and expansion of spread films on the LWSB and "*in situ*" FM. The increased liftoff area of the SP-B-containing film relative to those of the lipid–peptoid films is attributed to the sheer size of the molecule, which is present in the mixture in both monomer and dimer form. The *N*-terminus alkylation in **2** and **3** did not significantly alter liftoff when compared to **1**. Given that the base structural attributes of the helix remained largely unchanged upon alkylation, this result is strong evidence that the alkyl chains of the peptoids were well-incorporated into the lipid acyl chains of the film, translating to nearly the same area occupied per molecule at the interface.

Indications of superior surface activity upon alkylation are also present in the plateau regime (high π, low γ) of the compressed film, where alterations in the shape, size, and phase segregation morphology of the film are most evident. The very pronounced plateau of the SP-B-containing film demonstrates extensive structural reorganization and 3D folding of material, in and below the interfacial monolayer, which allows the film to reach high π without substantial loss of material to the subphase. Therefore, a change in shape or increase in plateau size, as demonstrated with **2** and **3**, points to an increase in biomimetic behavior relative to **1**. In addition, the decrease in LC domain size and increase in the density of small bright protrusions in FM images further suggests improvements in film organization and lipid insertion ability of the peptoids post-alkylation. Small LC domains are believed to minimize line tension at the phase boundaries and increase the feasibility of film refolding and re-spreading during increases or decreases in π, respectively.

The idea that temperature affects peptoid inclusion into the lipid film may be obvious given the increases in liftoff area and plateau size at higher temperature. However, upon film expansion, a marked phase transition or 'plateau' is present in lipid–peptoid films at lower temperature, which does not occur when SP-B is included. The transition may correspond to a different mechanism of reincorporating excluded peptoid or lipid–peptoid material as the available trough area increases; the increased bulkiness or rigidity of the aromatic-rich peptoid helix may hinder re-incorporation at lower temperature. Surprisingly, at 37 °C, near the T_c of the lipid film, the lipid–peptoid expansion isotherm 'plateaus' more closely resembled that of the TL + SP-B film. Because efficient reorganization and reincorporation of excluded material upon expansion directly relates to re-spreadability, they are considered critical features of LS films. The considerable 'plateau' changes in lipid–peptoid films with increasing temperature suggest that SP-B-containing film properties may still be superior; other structural attributes of SP-B are probably necessary in peptoids to achieve optimal film re-spreadability.

AFM imaging of the lipid–peptoid films demonstrated that, above the plateau surface tension regime, the presence of *N*-terminus alkylation afforded two differentiated regions in the AFM images, one of gel-like LC domains, and the other containing innumerous "nanosilos" that surrounded the LC domains. Notably, at higher surface pressure, TL + SP-B_{1-25} did not form nanosilos of considerable height, which may attest to its inferior surface activity relative to full-length SP-B. However, TL and TL + **1** formed nanosilo-like structures that were considerably higher than those previously observed for these films (~10–20 nm vs. ~5–8 nm in height) [74]. Interestingly, upon *N*-terminus peptoid alkylation, nanosilos formed in heights previously reported (~5–8 nm in height), and became smaller in diameter, more densely packed, and more homogeneous in size [74]. Furthermore, only the LC domains of TL + **3** retained similar shapes and sizes to

those observed at lower surface pressure. It can be hypothesized that numerous nanosilos of moderate height, closely linked to the interface, would be more easily reinserted upon expansion than larger, unevenly dispersed aggregates, and it appears that *N*-terminus peptoid dialkylation enhanced this effect to the largest degree. The presence of alkylated peptoid in the film therefore prevents one continuous gel-like interfacial film, with select aggregates, at higher surface pressure (TL), and instead creates a differentiated region containing interfacial components in the form of nanosilos. These nanosilos may improve the re-spreading properties of the film, allowing reinsertion of material when expansion occurs. Our results therefore agree with previous reports that suggest that nanosilos trap excluded material (likely POPG and peptoid/tide) from irreversible loss to the subphase, thus enhancing re-spreadability and ultimately increasing surface activity [74].

Protein/peptide lipidation has been employed by Nature and researchers to enhance biological activity [76,82–84]. Attaching a lipid-like chain facilitates interactions with lipid membranes, allows for intra- and intermolecular associations, and functions to mediate protein trafficking and stability. In this case, the question to be answered is what the role of SP-C-like *N*-terminus peptoid alkylation is once attached to an SP-B-like amphipathic peptoid helix. Our hypothesis for a molecular mechanism of action is outlined in the graphic of Fig. 9B. The alkylated chain(s) essentially function to extend the insertion region of **1**, thus ensuring that the molecule is attached to the interface, or remains predominantly lipid-associated. It is far-reaching to suggest that these simple amphipathic helices completely mimic the homodimerized natural SP-B dimer in its structure or function. The ability of these peptoids to mimic SP-C is even less likely, as the facially amphipathic patterning and lack of high hydrophobicity in the helix prohibit any possibility of spanning a lipid bilayer to sustain an attached surfactant reservoir. However, this alkylated amphipathic helix may be capable of remaining inserted into lipid moieties, transporting lipids to and from the interface, and in the case of **3**, connecting a monolayer and a bilayer through multiple alkylated chain 'anchors.' These molecular actions would increase adsorptive properties, reduce the surface tension, and enhance re-spreadability of the film.

The need for di- vs. monoalkylation was also addressed in this study, as **3** retained a lower γ_{max} during cycling (which was more stable than **2**, as evidenced by the decrease in σ (Table 2)), a more pronounced plateau on the LWSB, and increased nanosilo formation resulting in two differentiated regions in AFM images, relative to TL + **2**. Because a facially amphipathic helix would prefer to associate with the lipid headgroups and aqueous subphase, it is reasonable to speculate that dialkylation is necessary to fully anchor the insertion region into a lipid layer. Monoalkylation could permit conformational flexibility or intramolecular associations rather than incorporation into the lipid film. The decreased UV/Vis absorbance at ~260 nm of **2** relative to **3** may be an indication of this.

5. Concluding remarks

Ideally, the substitution of SP-B and/or SP-C in a biomimetic formulation with a single, fully functional biomimic would result in a bioavailable, cost-effective, and safe SRT alternative to animal-derived material [85,86]. Thus far, the investigation into biomimicry of SP-B and SP-C with peptoids has shown tremendous promise. We have presented solid evidence, through multiple *in vitro* surface activity tests in a tri-component lipid film, that *N*-terminus alkylation strikingly improves the surfactant activity of a single, aromatic, and amphipathic peptoid helix mimicking SP-B by improving the insertion ability of the peptoid into the fluid phase of the lipid film. A slight benefit in dialkylation vs. monoalkylation was also observed. These results imply that a similar strategy could be employed to augment the surface activity of single amphipathic helix peptide SP-B mimics that have, to date, failed to be efficacious enough for introduction to the pharmaceutical market. The synthesis of such *N*-terminus alkylated amphipathic helices, peptide or peptoid, is a feasible, cost-friendly, and much preferred alternative to generating mass quantities of dimerized or otherwise structurally complex SP-B-like mimics. We have further demonstrated that peptoid-based SP-B mimics do generally mimic the surface activity of SP-B by substantially improving interfacial adsorption, maintaining a reduced surface tension, and enhancing re-spreadability of lipid films. Further investigations into the properties of these molecules are definitely warranted, and cell toxicity studies and *in vivo* work are currently underway for this purpose. Through these additional studies, these functional, simple, easily synthesized, stable, and non-natural molecules may realize their full potential as surfactant protein mimics in an LS formulation.

Acknowledgements

AEB, SLSS, and MTD thank Jesús Pérez-Gil for kindly gifting isolated porcine-derived SP-B. AEB, SLSS, NJB, and MTD acknowledge Mark Johnson for PBS use. AEB and MTD acknowledge the Keck Biophysics Facility at NU for CD and UV/Vis use. This work was supported by the US National Institutes of Health (NIH Grant 2 R01 HL067984) and the US National Science Foundation (Grant BES-0101195 and Collaborative Research in Chemistry Grant CHE-0404704). NJB acknowledges support from the NIH Biotechnology Training Program Fellowship. JBS acknowledges support from a Lundbeck Foundation personal fellowship and the Forskningrådet for Natur og Universe grants from Luis A. Bagatolli that support the Membrane Biophysics and Biophotonics Group and associated facilities. JBS also gratefully acknowledges use of MEMPHYS-Center for Biomembrane Physics (Danish National Research Foundation Center of Excellence) and Adam C. Simonsen for AFM use.

Appendix A. Supplementary data

Supplementary Materials associated with this article can be found, in the online version, at doi:10.1016/j.bbamem.2010.04.012.

References

[1] L. Creuwels, L.M. van Golde, H.P. Haagsman, The pulmonary surfactant system: biochemical and clinical aspects, Lung 175 (1997) 1–39.
[2] J. Goerke, J.A. Clements, Alveolar surface tension and lung surfactant, The Handbook of Physiology, Sec. 3, The Respiratory System, The American Physiological Society, Bethesda, MD, vol. 3, 1986, pp. 247–262.
[3] R.H. Notter, Lung Surfactants: Basic Science and Clinical Applications, Marcel Dekker, New York, 2000.
[4] A.G. Serrano, J. Perez-Gil, Protein–lipid interactions and surface activity in the pulmonary surfactant system, Chem. Phys. Lipids 141 (2006) 105–118.
[5] S. Hawgood, K. Schiffer, Structures and properties of the surfactant-associated proteins, Annu. Rev. Physiol. 53 (1991) 375–394.
[6] J. Johansson, T. Curstedt, B. Robertson, The proteins of the surfactant system, Eur. Respir. J. 7 (1994) 372–391.
[7] S.B. Hall, A.R. Venkitaraman, J.A. Whitsett, B.A. Holm, R.H. Notter, Importance of hydrophobic apoproteins as constituents of clinical exogenous surfactants, Am. Rev. Respir. Dis. 145 (1992) 24–30.
[8] J. Pérez-Gil, K.M.W. Keough, Interfacial properties of surfactant proteins, Biochim. Biophys. Acta 1408 (1998) 203–217.
[9] Z.D. Wang, S.B. Hall, R.H. Notter, Roles of different hydrophobic constituents in the adsorption of pulmonary surfactant, J. Lipid Res. 37 (1996) 790–798.
[10] R. Veldhuizen, K. Nag, S. Orgeig, F. Possmayer, The role of lipids in pulmonary surfactant, Biochim. Biophys. Acta 1408 (1998) 90–108.
[11] M.E. Avery, J. Mead, Surface properties in relation to atelectasis and hyaline membrane disease, Am. J. Dis. Child. 97 (1959) 517–523.
[12] U. Pison, W. Seeger, R. Buchhorn, T. Joka, M. Brand, U. Obertacke, H. Neuhof, K.P. Schmit-Nauerburg, Surfactant abnormalities in patients with respiratory-failure after multiple trauma, Am. Rev. Respir. Dis. 140 (1989) 1033–1039.
[13] J.E. Lewis, A.H. Jobe, Surfactant and the adult respiratory distress syndrome, Am. Rev. Respir. Dis. 147 (1993) 218–233.

[14] B. Robertson, J. Johansson, T. Curstedt, Synthetic surfactants to treat neonatal lung disease, Mol. Med. Today 6 (2000) 119–124.
[15] O. Blanco, J. Pérez-Gil, Biochemical and pharmacological differences between preparations of exogenous natural surfactant used to treat respiratory distress syndrome: role of the different components in an efficient pulmonary surfactant, Eur. J. Pharmacol. 568 (2007) 1–15.
[16] F.R. Moya, A. Maturana, Animal-derived surfactants versus past and current synthetic surfactants: current status, Clin. Perinatol. 34 (2007) 145–177.
[17] K. Kirshenbaum, A.E. Barron, R.A. Goldsmith, P. Armand, E.K. Bradley, K.T.V. Truong, K.A. Dill, F.E. Cohen, R.N. Zuckermann, Sequence-specific polypeptoids: a diverse family of heteropolymers with stable secondary structure, Proc. Natl. Acad. Sci. U. S. A. 95 (1998) 4303–4308.
[18] C.W. Wu, S.L. Seurynck, K.Y.C. Lee, A.E. Barron, Helical peptoid mimics of lung surfactant protein C, Chem. Biol. 10 (2003) 1057–1063.
[19] S.L. Seurynck, J.A. Patch, A.E. Barron, Simple, helical peptoid analogs of lung surfactant protein B, Chem. Biol. 12 (2005) 77–88.
[20] S.L. Seurynck-Servoss, M.T. Dohm, A.E. Barron, Effects of including an N-terminal insertion region and arginine-mimetic side chains in helical peptoid analogues of lung surfactant protein B, Biochemistry 45 (2006) 11809–11818.
[21] S.L. Seurynck-Servoss, N.J. Brown, M.T. Dohm, C.W. Wu, A.E. Barron, Lipid composition greatly affects the in vitro surface activity of lung surfactant protein mimics, Colloids Surf., B Biointerfaces 57 (2007) 37–55.
[22] N.J. Brown, C.W. Wu, S.L. Seurynck-Servoss, A.E. Barron, Effects of hydrophobic helix length and side chain chemistry on biomimicry in peptoid analogues of SP-C, Biochemistry 47 (2008) 1808–1818.
[23] M.T. Dohm, S.L. Seurynck-Servoss, J. Seo, R.N. Zuckermann, A.E. Barron, Close mimicry of lung surfactant protein B by "clicked" dimers of helical, cationic peptoids, Biopolymers (Peptide Sci.) 92 (2009) 538–553.
[24] R.N. Zuckermann, J.M. Kerr, S.B.H. Kent, W.H. Moos, Efficient method for the preparation of peptoids oligo(N-substituted glycines) by submonomer solid-phase synthesis, J. Am. Chem. Soc. 114 (1992) 10646–10647.
[25] T.J. Sanborn, C.W. Wu, R.N. Zuckermann, A.E. Barron, Extreme stability of helices formed by water-soluble poly-N-substituted glycines (polypeptoids) with alpha-chiral side chains, Biopolymers 63 (2002) 12–20.
[26] C.W. Wu, T.J. Sanborn, R.N. Zuckermann, A.E. Barron, Peptoid oligomers with alpha-chiral, aromatic side chains: effects of chain length on secondary structure, J. Am. Chem. Soc. 123 (2001) 2958–2963.
[27] P. Armand, K. Kirshenbaum, R.A. Goldsmith, S. Farr-Jones, A.E. Barron, K.T.V. Truong, K.A. Dill, D.F. Mierke, F.E. Cohen, R.N. Zuckermann, E.K. Bradley, NMR determination of the major solution conformation of a peptoid pentamer with chiral side chains, Proc. Natl. Acad. Sci. U. S. A. 95 (1998) 4309–4314.
[28] C.W. Wu, K. Kirshenbaum, T.J. Sanborn, J.A. Patch, K. Huang, K.A. Dill, R.N. Zuckermann, A.E. Barron, Structural and spectroscopic studies of peptoid oligomers with alpha-chiral aliphatic side chains, J. Am. Chem. Soc. 125 (2003) 13525–13530.
[29] M. Andersson, T. Curstedt, H. Jornvall, J. Johansson, An amphipathic helical motif common to tumourolytic polypeptide NK-Lysin and pulmonary surfactant polypeptide SP-B, FEBS Lett. 362 (1995) 328–332.
[30] S. Hawgood, M. Derrick, F. Poulain, Structure and properties of surfactant protein B, Biochim. Biophys. Acta 1408 (1998) 150–160.
[31] S. Zaltash, M. Palmblad, T. Curstedt, J. Johansson, B. Persson, Pulmonary surfactant protein B: a structural model and a functional analogue, Biochim. Biophys. Acta 1466 (2000) 179–186.
[32] H.P. Haagsman, R.V. Diemel, Surfactant-associated proteins: functions and structural variation, Comp. Biochem. Physiol. A. Mol. Integr. Physiol. 129 (2001) 91–108.
[33] G. Vandenbussche, A. Clercx, M. Clercx, T. Curstedt, J. Johansson, H. Jornvall, J.M. Ruysschaert, Secondary structure and orientation of the surfactant protein SP-B in a lipid environment — a Fourier-transform infrared-spectroscopy study, Biochemistry 31 (1992) 9169–9176.
[34] A. Waring, H.W. Taeusch, R. Bruni, J.D. Amirkhanian, B.R. Fan, R. Stevens, J. Young, Synthetic amphipathic sequences of surfactant protein-B mimic several physicochemical and *in vivo* properties of native pulmonary surfactant proteins, Pept. Res. 2 (1989) 308–313.
[35] R. Bruni, H.W. Taeusch, A.J. Waring, Surfactant protein-B–lipid interactions of synthetic peptides representing the amino-terminal amphipathic domain, Proc. Natl. Acad. Sci. U. S. A. 88 (1991) 7451–7455.
[36] J.E. Baatz, V. Sarin, D.R. Absolom, C. Baxter, J.A. Whitsett, Effects of surfactant-associated protein SP-B synthetic analogs on the structure and surface-activity of model membrane bilayers, Chem. Phys. Lipids 60 (1991) 163–178.
[37] L.M. Gordon, S. Horvath, M.L. Longo, J.A.N. Zasadzinski, H.W. Taeusch, K. Faull, C. Leung, A.J. Waring, Conformation and molecular topography of the N-terminal segment of surfactant protein B in structure-promoting environments, Protein Sci. 5 (1996) 1662–1675.
[38] L.M. Gordon, K.Y.C. Lee, M.M. Lipp, J.A. Zasadzinski, F.J. Walther, M.A. Sherman, A.J. Waring, Conformational mapping of the N-terminal segment of surfactant protein B in lipid using C-13-enhanced Fourier transform infrared spectroscopy, J. Pept. Res. 55 (2000) 330–347.
[39] C.G. Cochrane, S.D. Revak, Pulmonary surfactant protein-B (SP-B)–structure-function-relationships, Science 254 (1991) 566–568.
[40] E.J.A. Veldhuizen, A.J. Waring, F.J. Walther, J.J. Batenburg, L.M.G. van Golde, H.P. Haagsman, Dimeric N-terminal segment of human surfactant protein B (dSP-B1-25) has enhanced surface properties compared to monomeric SP-B1-25, Biophys. J. 79 (2000) 377–384.
[41] A.J. Waring, F. Walther, L.M. Gordon, J. Hernandez-Juviel, T. Hong, M.A. Sherman, C. Alonso, T. Alig, J.W. Brauner, D. Bacon, J. Zasadzinski, The role of charged amphipathic helices in the structure and function of surfactant protein B, J. Pept. Res. 66 (2005) 364–374.
[42] J. Johansson, T. Szyperski, T. Curstedt, K. Wuthrich, The NMR structure of the pulmonary surfactant-associated polypeptide SP-C in an apolar solvent contains a valyl-rich α-helix, Biochemistry 33 (1994).
[43] L.A. Creuwels, E.H. Boer, R.A. Demel, L.M.G. van Golde, H.P. Haagsman, Neutralization of the positive charges of surfactant protein C: effects on structure and function, J. Biol. Chem. 270 (1995) 16225–16229.
[44] A. Kramer, A. Wintergalen, M. Sieber, H.J. Galla, M. Amrein, R. Guckenberger, Distribution of the surfactant-associated protein C within a lung surfactant model film investigated by near-field optical microscopy, Biophys. J. 78 (2000) 458–465.
[45] X.H. Bi, C.R. Flach, J. Perez-Gil, I. Plasencia, D. Andreu, E. Oliveira, R. Mendelsohn, Secondary structure and lipid interactions of the N-terminal segment of pulmonary surfactant SP-C in Langmuir films: IR reflection–absorption spectroscopy and surface pressure studies, Biochemistry 41 (2002) 8385–8395.
[46] C. Alonso, A. Waring, J.A. Zasadzinski, Keeping lung surfactant where it belongs: protein regulation of two-dimensional viscosity, Biophys. J. 89 (2005) 266–273.
[47] P.N. Nakorn, M.C. Meyer, C.R. Flach, R. Mendelsohn, H.J. Galla, Surfactant protein C and lung function: new insights into the role of alpha-helical length and palmitoylation, Eur. Biophys. J. 36 (2007) 477–489.
[48] I. Plasencia, F. Baumgart, D. Andreu, D. Marsh, J. Perez-Gil, Effect of acylation on the interaction of the N-terminal segment of pulmonary surfactant protein SP-C with phospholipid membranes, Biochim. Biophys. Acta 1778 (2008) 1274–1282.
[49] T. Takei, Y. Hashimoto, T. Aiba, K. Sakai, T. Fujiwara, The surface properties of chemically synthesized peptides analogous to human pulmonary surfactant protein C, Biol. Pharm. Bull. 19 (1996) 1247–1253.
[50] M. Ikegami, A.H. Jobe, Surfactant protein-C in ventilated premature lamb lung, Pediatr. Res. 44 (1998) 860–864.
[51] G. Nilsson, M. Gustafsson, G. Vandenbussche, E. Veldhuizen, W.J. Griffiths, J. Sjovall, H.P. Haagsman, J.M. Ruysschaert, B. Robertson, T. Curstedt, J. Johansson, Synthetic peptide-containing surfactants — evaluation of transmembrane versus amphipathic helices and surfactant protein C poly-valyl to poly-leucyl substitution, Eur. J. Biochem. 255 (1998) 116–124.
[52] S. Hawgood, A. Ogawa, K. Yukitake, M. Schlueter, C. Brown, T. White, D. Buckley, D. Lesikar, B.J. Benson, Lung function in premature rabbits teated with recombinant human surfactant protein C, Am. J. Respir. Crit. Care Med. 154 (1996) 484–490.
[53] D. Lukovic, I. Plasencia, F.J. Taberner, J. Salgado, J.J. Calvete, J. Perez-Gil, I. Mingarro, Production and characterisation of recombinant forms of human pulmonary surfactant protein C (SP-C): structure and surface activity, Biochim. Biophys. Acta 1758 (2006) 509–518.
[54] Y. Tanaka, T. Takei, T. Aiba, K. Masuda, A. Kiuchi, T. Fujiwara, Development of synthetic lung surfactants, J. Lipid Res. 27 (1986) 475–485.
[55] N.J. Brown, J. Johansson, A.E. Barron, Biomimicry of surfactant protein C, Acc. Chem. Res. 41 (2008) 1409–1417.
[56] A. Blume, A comparative study of the phase transitions of phospholipid bilayers and monolayers, Biochim. Biophys. Acta 557 (1979) 32–44.
[57] D. Marsh, Lateral pressure in membranes, Biochim. Biophys. Acta 1286 (1996) 183–223.
[58] J. Perez-Gil, A. Cruz, C. Casals, Solubility of hydrophobic surfactant proteins in organic solvent/water mixtures. Structural studies on SP-B and SP-C in aqueous organic solvents and lipids, Biochim. Biophys. Acta 1168 (1993) 261–270.
[59] R.B. Merrifield, Solid phase peptide synthesis. I. the synthesis of a tetrapeptide, J. Am. Chem. Soc. 85 (1963) 2149–2154.
[60] I. Plasencia, A. Cruz, C. Lopez-Lacomba, C.R. Flach, J. Perez-Gil, Selective labeling of pulmonary surfactant protein SP-C in organic solution, Anal. Biochem. 296 (2001) 49–56.
[61] F. Bringezu, J.Q. Ding, G. Brezesinski, A.J. Waring, J.A. Zasadzinski, Influence of pulmonary surfactant protein B on model lung surfactant monolayers, Langmuir 18 (2002) 2319–2325.
[62] F. Bringezu, J.Q. Ding, G. Brezesinski, J.A. Zasadzinski, Changes in model lung surfactant monolayers induced by palmitic acid, Langmuir 17 (2001) 4641–4648.
[63] S.L. Seurynck, N.J. Brown, C.W. Wu, K.W. Germino, E.K. Kohlmeir, E.P. Ingenito, M. R. Glucksberg, A.E. Barron, M. Johnson, Optical monitoring of bubble size and shape in a pulsating bubble surfactometer, J. Appl. Physiol. 99 (2005) 624–633.
[64] S.L. Frey, L. Pocivavsek, A.J. Waring, F.J. Walther, J.M. Hernandez-Juviel, P. Ruchala, K.Y.C. Lee, Functional importance of the NH2-terminal insertion sequence of lung surfactant protein B, Am. J. Physiol. Lung Cell Mol. Physiol. 298 (2010) L335–L347.
[65] G. Putz, J. Goerke, H.W. Taeusch, J.A. Clements, Comparison of captive and pulsating bubble surfactometers with use of lung surfactants, J. Appl. Physiol. 76 (1994) 1425–1431.
[66] J. Bernardino de la Serna, J. Pérez-Gil, A.C. Simonsen, L.A. Bagatolli, Cholesterol rules: direct observation of the coexistence of two fluid phases in native pulmonary surfactant membranes at physiological temperatures, J. Biol. Chem. 279 (2004) 40715–40722.
[67] M.I. Angelova, S. Soleau, P. Meleard, J.F. Faucon, P. Bothorel, Preparation of giant vesicles by external AC electric fields, Prog. Colloid & Polym. Sci. 89 (1992) 127–131.
[68] M.I. Angelova, D.S. Dimitrov, Liposome electroformation, Faraday Discuss. Chem. Soc. 81 (1986) 303–311.
[69] M.L. Fidorra, L. Duelund, C. Leidy, A.C. Simonsen, L.A. Bagatolli, Absence of fluid-ordered/fluid-disordered phase coexistence in ceramide/POPC mixtures containing cholesterol, Biophys. J. 90 (2006) 4437–4451.
[70] A.G. Serrano, M.A. Ryan, T.E. Weaver, J. Pérez-Gil, Critical structure-function determinants within the N-terminal region of pulmonary surfactant protein B, Biophys. J. 90 (2006) 238–249.

[71] N.J. Brown, J. Bernardino de la Serna, A.E. Barron, N-terminal alkylation significantly improves biomimicry of a peptoid analogue of surfactant protein C, Biophys. J. in revision (2010)
[72] A. Cruz, L. Vazquez, M. Velez, J. Pérez-Gil, Effect of pulmonary surfactant protein SP-B on the micro- and nanostructure of phospholipid films, Biophys. J. 86 (2004) 308–320.
[73] T. Baumgart, G. Hunt, E.F. Farkas, W.W. Webb, G.W. Feigenson, Fluorescence probe partitioning between Lo/Ld phases in lipid membranes, Biochim. Biophys. Acta 1768 (2007) 2182–2194.
[74] J.Q. Ding, I. Doudevski, H.E. Warriner, T. Alig, J.A. Zasadzinski, Nanostructure changes in lung surfactant monolayers induced by interactions between palmitoyloleoylphosphatidylglycerol and surfactant protein B, Langmuir 19 (2003) 1539–1550.
[75] P. Forns, J.L. Lauer-Fields, S. Gao, G.B. Fields, Induction of protein-like architecture by monoalkyl hydrocarbon chains, Biopolymers (Peptide Sci.) 54 (2000) 531–546.
[76] G.B. Fields, J.L. Lauer, Y. Dori, P. Forns, Y.-C. Yu, M. Tirrell, Proteinlike molecular architecture: biomaterial application for inducing cellular receptor binding and signal transduction, Biopolymers (Peptide Sci.) 47 (1998) 143–151.
[77] R. Thomas, The denaturation of DNA, Gene 135 (1993) 77–79.
[78] R.W. Walters, R.R. Jenq, S.B. Hall, Distinct steps in the adsorption of pulmonary surfactant to an air–liquid interface, Biophys. J. 78 (2000) 257–266.
[79] A. Saenz, O. Canadas, L.A. Bagatolli, M.E. Johnson, C. Casals, Physical properties and surface activity of surfactant-like membranes containing the cationic and hydrophobic peptide KL4, FEBS J. 273 (2006) 2515–2527.
[80] J. Perez-Gil, Structure of pulmonary surfactant membranes and films: the role of proteins and lipid–protein interactions, Biochim. Biophys. Acta 1778 (2008) 1676–1695.
[81] Y.Y. Zuo, R.A.W. Veldhuizen, A.W. Neumann, N.O. Petersen, F. Possmayer, Current perspectives in pulmonary surfactant — inhibition, enhancement and evaluation, Biochim. Biophys. Acta 1778 (2008) 1947–1977.
[82] D. Avrahami, Y. Shai, Bestowing antifungal and antibacterial activities by lipophilic acid conjugation to D,L-amino acid-containing antimicrobial peptides: a plausible mode of action, Biochemistry 42 (2003) 14946–14956.
[83] M.J. Nadolski, M.E. Linder, Protein lipidation, FEBS J. 274 (2007) 5202–5210.
[84] A.F. Chu-Kung, K.N. Bozzelli, N.A. Lockwood, J.R. Haseman, K.H. Mayo, M. Tirrell, Promotion of peptide antimicrobial activity by fatty acid conjugation, Bioconj. Chem. 15 (2004) 530–535.
[85] I. Mingarro, D. Lukovic, M. Vilar, J. Pérez-Gil, Synthetic pulmonary surfactant preparations: new developments and future trends, Curr. Med. Chem. 15 (2008) 393–403.
[86] C.W. Wu, A.E. Barron, Biomimetic lung surfactant replacements, in: A.K. Dillow (Ed.), Biomimetic Materials and Design, Marcel-Dekker, New York, 2002, pp. 565–633.